# Investigation into the shear property of thin-walled additively manufactured structures using staggered fused filament fabrication

**Thomas Romeijn[a b*], Brooke Wells[b], Dongbin Wei[b] and Gavin Paul[b]**

[a] Mineral Technologies, 11 Elysium Road, Carrara QLD 4211, Australia
[b] Faculty of Engineering and Information Technology, University of Technology Sydney, NSW 2007, Australia
*Phone number: +61 7 5569 1300, E-mail: Thomas.Romeijn@mineraltechnologies.com.au

## Abstract –

**Additive manufacturing techniques, such as Fused Filament Fabrication (FFF), are rapidly revolutionising the manufacturing and mining sectors. This paper presents an investigation into the shear behaviour of thin-walled FFF structures, printed via a proposed 'offset method'. Firstly, an alternative method of filament positioning in material extrusion is proposed, referred to as the 'offset method', which aims to reduce the volume of empty cavities between deposited material. Then the shear properties, density properties, and cross-sectional void surface area are compared to structures printed using the aligned printing method. Experimental results on solid printed (no infill) samples, through four different-sized nozzles, have shown the newly proposed method produces a 6.5% increase in density and a 7.2% improvement in maximum in-plane shear stress per millimetre increase in nozzle size, compared with the aligned method of FFF. The offset method was found to produce a material with increased interlayer contact, compared to the aligned method, which results in a higher fictitious shear stress modulus. The effect of the increased interlayer contact on the fictitious shear modulus and real shear stress was investigated using a FEM analysis of the unit cells. In short, using the same feedstock material, the offset method produces a stiffer material with a higher fictitious shear strength than the aligned method of FFF printing.**

## Keywords –

**Fused Filament Fabrication (FFF), Porosity, Density, Shear strength**

# 1 Introduction

Parts produced by the additive manufacturing process have evolved, in recent years, from mere conceptual visualisation aids to consumer-ready parts. The flexibility allowed by the additive manufacturing process relaxes the manufacturing constraints on a component design and as such, enables more design freedom in the shape of components. Thus, parts can be designed, or retrospectively redesigned, with far less geometrical restrictions than traditional manufacturing processes would impose.

Still, no process is without its limitations and when focussing on the most widely used additive manufacturing process, the Fused Filament Fabrication (FFF) technique, the extent of the design envelope is worth exploring. The smallest possible wall thickness in FFF is determined by several aspects. Naturally, the smallest wall thickness would be the thickness of a single extruded filament which in turn depends on the nozzle size used. Although a reduction in nozzle size would allow for a reduction in wall thickness, small nozzle sizes increase the build process time as the nozzle size determines the material extrusion rate [1]. Additionally, the thinnest possible wall thickness of structures for use in consumer-ready products must robustly withstand the forces imposed on them. The above makes it clear that the design of thin-walled customer-ready parts produced through FFF includes consideration of the material properties, with a focus on nozzle size selection, print time requirements and careful assessment of the forces the structure needs to withstand.

One challenge regarding the mechanical properties for FFF structures is that the nature of the production method can vary, in particular the non-uniform distribution of the feedstock. The FFF build process means that the final printed object is distinctly anisotropic even when an isotropic feedstock is deposited. Several research teams [2-4] have pointed out the orthotropic nature of the FFF process where, for different material properties in mutual orthogonal planes, the direction perpendicular to the build plane is the weakest. The material properties of the final print are thus determined by both the feedstock and build process [5]. This basic principle is further complicated by the vast number of process parameters that can be varied before and during material extrusion 3D printing.

The most critical parameters that affect the strength of a printed part, as determined by Lee et al. [6] and Sood et al. [7], are listed in the first column of Table 1 and some are visualised in Figure 1. Due to a lack of unified terminology in the field, alternative terms are given in brackets where applicable. There has been a considerable research effort to assess the effects of these variables on the strength of FFF structures and Dizon et al. [8] provides an extensive overview.

| **Process parameters affecting mechanical properties of FFF structures** | **Value in solid part printing** |
|---|---|
| Air gap (raster to raster air gap) | No air gap |
| Road width (bead width / filament width) | Variable but neighbouring roads will fuse together if the air gap is zero |
| Raster angle (raster fill angle / raster orientation) | Single direction |
| Number of contours (number of shells) | No contours |
| Infill (raster pattern) | No infill |
| Layer thickness (slice thickness, slice height) | Variable |
| Build orientation (build direction / part print direction) | Walls assumed perpendicular to the X-Y plane of Figure 1 |

**Table 1: Process parameters affecting mechanical properties of FFF structures and their settings when applied to solid part printing.**

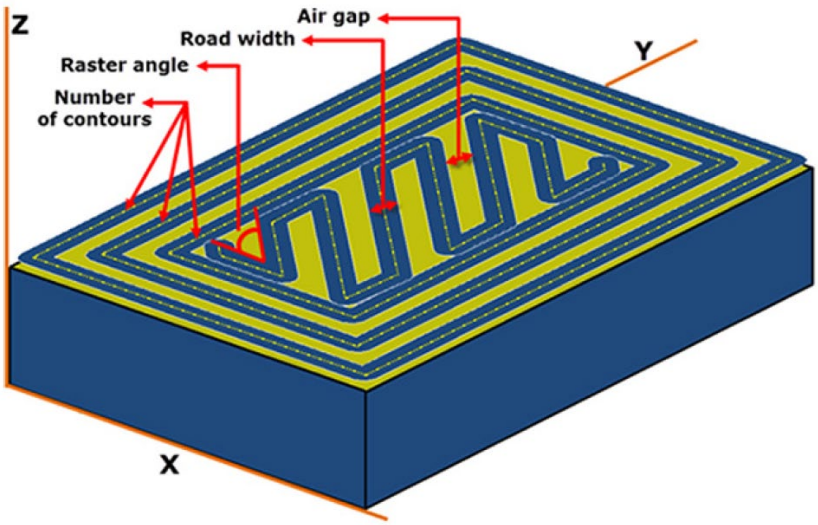


**Figure 1: Visualisation of process parameters affecting mechanical properties [9].**

In order to search for the smallest practical wall thickness several assumptions can be made. Practical thin-wall structures produced through FFF are likely to be only several roads thick. As such, the thinnest walls cannot accommodate intricate infill patterns which in turn negates the use of contours. Furthermore, thin walls perpendicular to the build surface, the X-Y plane of Figure 1, would not be able to utilise different raster angels as the print head commonly moves in a plane parallel to the build surface. It follows that when the thinnest practical wall thickness is desired, a printed part should be assumed with roads running in a single direction in the build surface plane where only the road width and layer thickness can be varied. Such a print, henceforth referred to as a 'solid print', converts several of the parameters listed in Table 1 to fixed values, as shown in the right-hand column of the table.

Several studies deal with comparable solid prints while assessing the strength of the printed samples [10-13]. As shown in Figure 3, Montero et al. [14] found that the tensile properties of FFF printed samples with parallel printed roads in the same direction across all layers, referred to as the 0° print, is superior in strength compared to the alternating raster angle combinations, e.g. 0°/90°, 45°/-45°. These findings are not surprising as the tensile load aligns with the direction of the roads in this case. The alternative solid print, where all roads are parallel across all layers but angled perpendicular to the load vector, labelled as the 90° print, can be seen in Figure 3 as the weakest option that was tested. Dizon et al. [8] found that the weak interlayer bonding causes the poor performance of such a print under tension.

Tensile failure of parts produced through FFF were investigated by Casavola et al. [4]. The researchers showed that the failure behaviour differs when the samples were printed in the 0°, 45° or 90° direction. Pure brittle failure is dominant in a 90° print whereas plastic deformation before failure was found in a 0° printed sample, refer Figure 2. Moreover, the researchers highlighted the disparity between strength properties of the feedstock wire and those of the printed sample even for the most ideal, load-aligned (0°) printing settings.

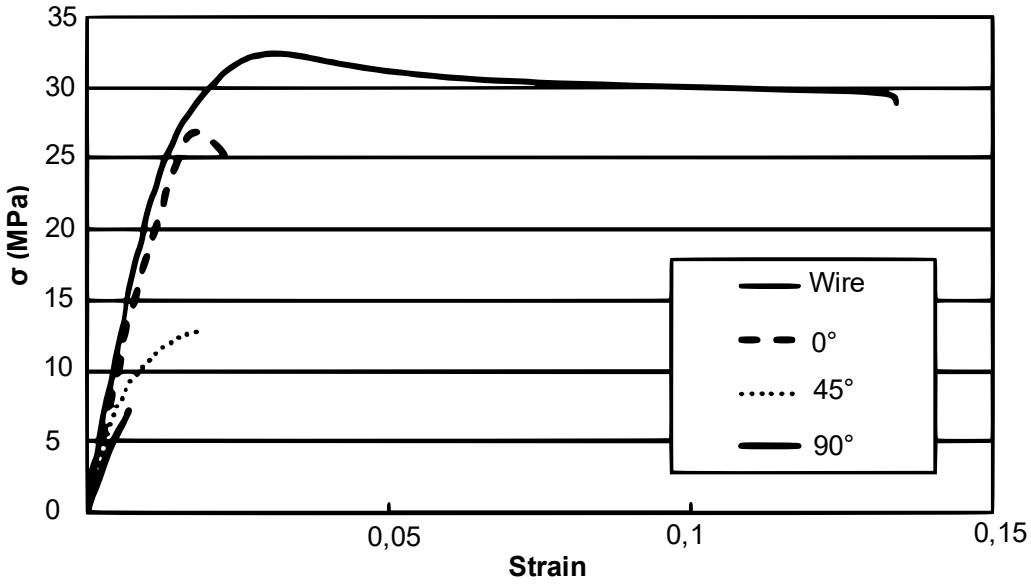


**Figure 2: Representative tensile testing data for ABS at each raster orientation [4].**

Susmel & Ahmed [15] applied the Theory of Critical Distances (TCD) to PLA samples produced through FFF to assess their static strength and fracture behaviour in both tensile and three-point bending. Surprisingly, the researchers found that the sharpest geometric features, or largest stress raisers, did not consistently produce to the lowest static strength of the sample as a whole. In a subsequent article [16] the researchers extended the TCD method to samples which included voids and introduced a stress measure which includes both the voids and the contact area between roads. They determined the fictitious failure strength, the 0.2% fictitious proof stress, and the fictitious elastic modulus E of their material. The researchers showed these three material properties decreased rapidly when voids sizes were increased. Aliheidari et al. [17] further investigated fracture of 100% infill ABS samples with roads in a single direction for a 0.35mm nozzle size. The researchers showed that the void size was reduced with increasing nozzle temperature (210°C, 230°C and 240°C). The interlayer fracture resistance was found to increase with nozzle temperature as that allows higher polymer-chain mobility and increased time for inter-layer diffusion resulting in a stronger interlayer bond. When printing ABS at a nozzle temperature of 240°C, the near-perfect interlayer bonding was found as the fracture toughness resembled that of bulk ABS.

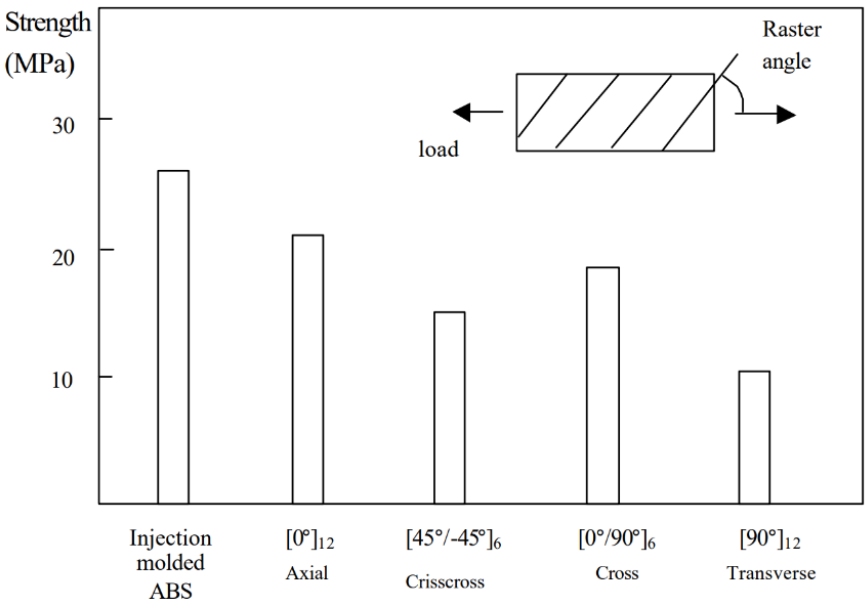


**Figure 3: Comparison of raster angle versus strength [14].**

Solid printed components loaded in shear perpendicular to the road direction also stress the relatively weak interlayer bonds. This topic was investigated by Zhang et al. [18] where the interfacial bonding strength of printed ABS samples was assessed, with a focus on layer thickness. The authors concluded that an increase in layer thickness negatively affected the shear strength, but only samples of the 45°/-45° stacking sequence were tested. Caminero et al. [19] compared the shear properties of continuous fibre-reinforced nylon printed through FFF to the unreinforced version. In that study, the samples used in the shear test were printed in the 90° direction only. For the neat unreinforced samples, the authors confirmed that increasing the layer thickness (0.1mm, 0.125mm and 0.2mm) caused a decrease in shear strength. They also showed that this effect was due to the increased void size, and thus porosity within the material. Thinner layers were found to fill voids more readily, thereby reducing porosity, which resulted in a higher shear strength compared to thickly layered samples. Cuan-Urquizo [3] investigated shear behaviour of FDM printed parts with regularly spaced voids that originated form their 'woodpile' stacking method. The researchers showed that in modelling shear behaviour the overlap of roads was essential to be accounted for.

A common method of material extrusion 3D printing is to deposit a layer of filaments directly on top of the previous layer (left image in Figure 4), henceforth referred to as the 'aligned method'. The finding of Zhang et al. [18], that an increase in layer thickness results in a decrease in shear strength, combined with the findings from Caminero et al. [19], that this effect was caused by an increased porosity with growing layer thicknesses, inspired a proposed alternative method of FFF, as shown in the right image in Figure 3. This novel way of FFF, devised by the authors of this paper, is henceforth referred to as the 'offset method' and is hypothesised to have reduced porosity, and thus superior shear properties compared to the aligned method.

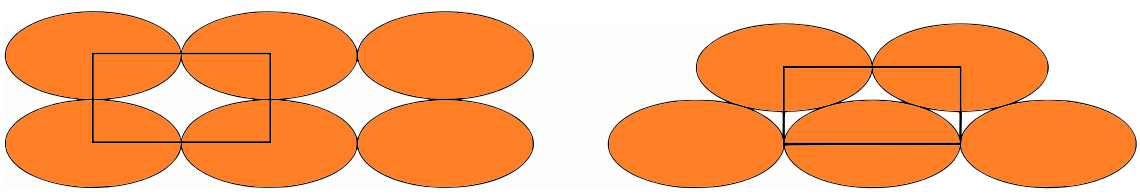

**Figure 4: The aligned FFF method (left) and the proposed offset FFF method (right). Black rectangles are the unit cells for each method.**

To progress the development of thin-walled 3D printed components, this paper will compare the offset FFF method to the aligned FFF method using shear strength as a metric to determine if the offset method indeed provides an improved shear performance. To the best of this research team's knowledge, no research to date has proposed a staggered method of FFF such as the offset method, and as such no study has been conducted into the effects of offsetting successive layers within a structure produced through FFF.

The paper is organised as follows. Section 2 will discuss the benefits and drawbacks of the offset method, materials, samples and test methodology used to assess the offset method. The experimental results and their impact are detailed in Section 3. The conclusion is described in Section 4.

## 2 Materials and Methods

### 2.1 Benefits and drawbacks of the offset method

It can be shown mathematically that a unit road cell, a square containing a complete oval road cross-section (shown in Figure 4), contains more feedstock per cross-sectional surface area in the offset method compared to that of the aligned printing technique. The unit road cells and their filament content are shown in Figure 5. As such, the offset method theoretically contains $4/2\sqrt{3}$ times, and thus 15.5% more feedstock than the aligned method. In this theoretical and idealised model, the viscous nature of the deposited filament and resulting road overlap is obviously ignored. Still, it can be reasonably assumed that a printing method where smaller voids are to be filled by a solidifying material would result in a less porous structure when compared to a printing method with larger void sizes. This applies even if a theorical contact point instead of a contact line is assumed. Thus, an expected benefit is that the additional material per unit road cell should improve the shear properties.

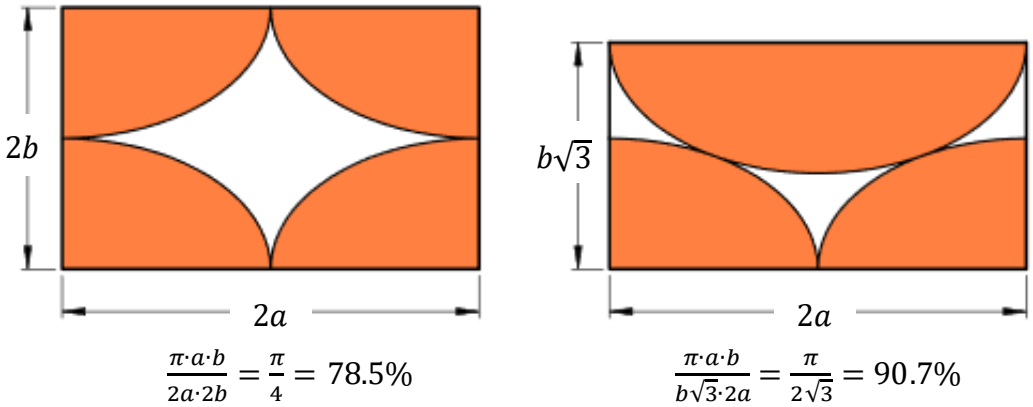


**Figure 5: The feedstock content of a unit road cell for both FFF methods, where $a$ is the long radius and $b$ is the short radius of the oval.**

If the increased density does show to improve the shear properties for the same road width, the inverse approach could be pursued as well: increase the layer thickness of the offset method until the same shear strength value as the aligned method is achieved. This approach would produce a print with equivalent shear properties to the aligned FFF method but with a larger layer thickness. As a larger nozzle size leads to an increase in extrusion rate, a beneficial reduction in build cycle time would follow.

From a broader material extrusion additive manufacturing perspective, this denser material deposition, combined with improved shear characteristics, would make the offset method more

suitable for the 3D printing of shear-dominated structures. This is advantageous where the addition of feedstock to improve the shear characteristic is undesirable, e.g. thin-walled structures.

One straightforward drawback of the offset printing method is the increased difficulty of the slicing code. Furthermore, Anitha et al. [20] showed, that an increase in layer thickness resulted in an increase in surface roughness. The offset method can be expected to have a similar detrimental effect and this will be more pronounced on the vertical faces of a printed structure due to the shifted horizontal layers.

To assess the possible benefits of the offset method, its density and shear properties will be compared to that of the aligned method of FFF. To fully capture the offset method, the above two comparisons will be done for four different nozzle sizes. Additionally, the difference in void surface area between the two methods will be determined via microscopic imaging techniques for a representative nozzle size.

### 2.2 Shear testing standard

Currently, no unified standard exists for the testing of structures produced via additive manufacturing [8, 13, 19, 21]. Various research groups have therefore utilised other standards that closely relate regarding the desired material properties. Zhang et al. [18] used an in-plane shear test in accordance to ASTM D3518 [22], but this standard is geared towards a 45°/-45° laminate, and as such not deemed applicable to the samples used in this study. ASTM D3846 [23], another shear standard, sees the compression of a double notched flat sample in a support jig, as shown in Figure 6. This standard will be utilised in this research paper. As such a jig is not self-supporting, a base is required according to the Boeing Specification Support Standard 7260 [24] to position the jig vertically which is also shown in the bottom right image of Figure 6.

When compressed, the sample will shear along a plane located between the two notches. The standard calls for these notches to be machined into a bar-shaped sample but the notches will be included in the printed test specimen for this series of tests. When included, the end of each notch will have to be defined by an FFF layer. This aspect will ensure the shear plane will be located in between two layers and it is exactly this interlayer connection where the lowest shear strength is expected to occur. A machined cut made in a 3D printed sample could result in a shear plane located internally to a layer, which is undesirable in this case.

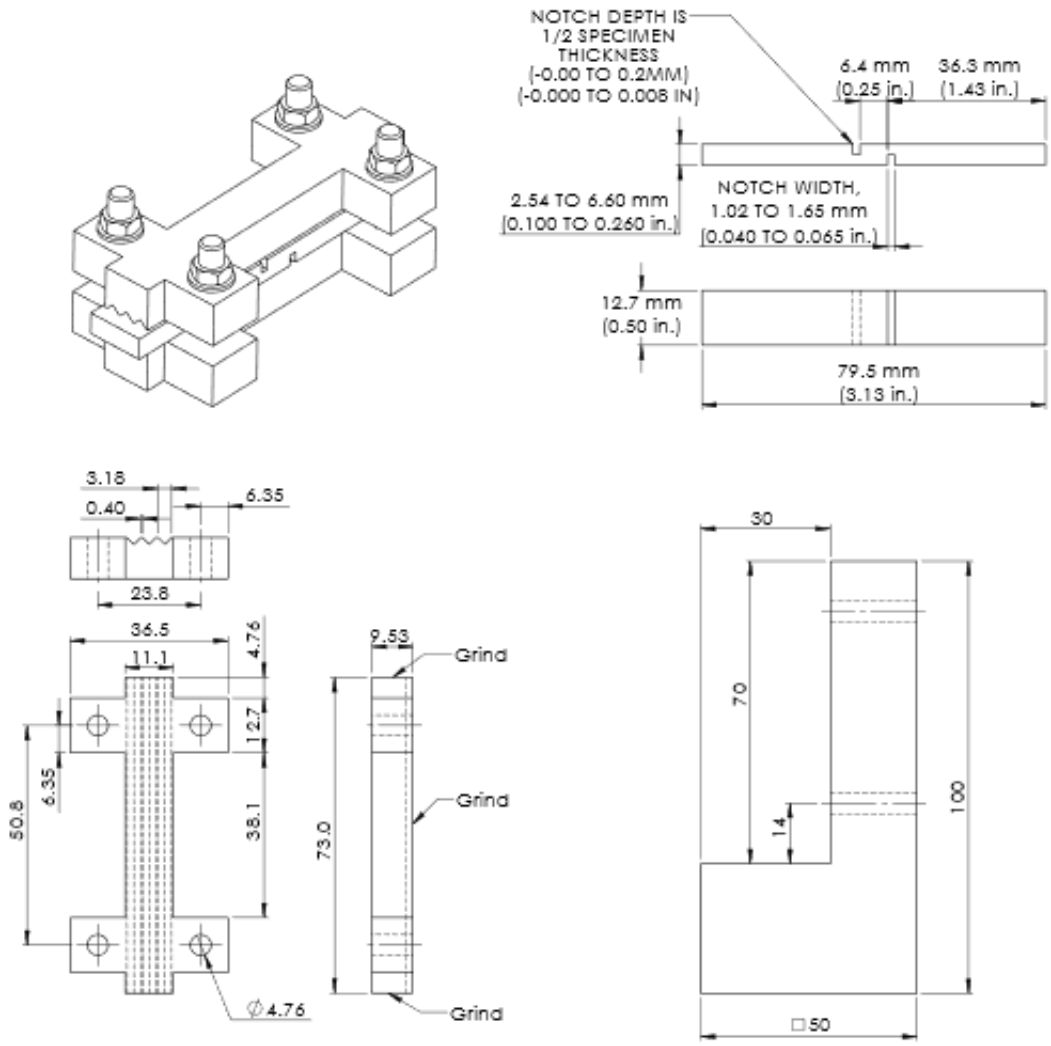


**Figure 6: The double notch sample and support jig [24, 25] (machining tolerance ±0.2mm where not indicated)**

## 2.3 Fabrication of shear and density samples

The samples were printed in ABS on a Creality CR-10 printer. ABS juice, a combination of acetone and ABS, was required to get the appropriate adhesion to the build platform. A temperature-controlled build volume has been used to further ease the 3D printing process. The fixed value of the process parameters used in the sample production are listed in Table 2, where some parameters depend on the nozzle size.

| Process parameters | Nozzle size | | | |
|---|---|---|---|---|
| | 0.3mm | 0.9mm | 1.2mm | 1.5mm |
| **Road width** | 0.2mm | 0.6mm | 0.8mm | 1mm |
| **Layer thickness (Aligned Method)** | 0.2mm | 0.6mm | 0.8mm | 1mm |
| **Layer thickness (Offset Method)** | 0.173mm | 0.52mm | 0.69mm | 0.87mm |
| **Nozzle temperature** | 250°C | 250°C | 255°C | 260°C |
| **Print bed temperature** | 100°C | | | |
| **Print speed** | 2400mm/min | | | |
| **Air gap** | No air gap, solid print | | | |
| **Raster angle** | Uniformly parallel to the width of the sample (i.e. the 12.7mm dimension in Figure 6) | | | |
| **Number of contours** | No contours | | | |
| **Infill** | No internal topology. The roads are uniformly parallel throughout the sample | | | |
| **Build orientation** | Largest sample face touching the print bed | | | |
| **ABS Brand** | Blueprinted | | | |
| **Density** | 1.05g/cm$^3$ | | | |
| **Ultimate tensile strength** | 45MPa | | | |

**Table 2: Process parameters affecting mechanical properties of FFF structures and their settings when applied to the test samples.**

Initial samples that were produced showed a significant degree of feedstock accumulation at the start and end of each road. The resulting local change in thickness could interfere with the support jig and was therefore machined away (refer Figure 7). The machining step consisted of firstly machining the top and bottom of each sample using a mill with a 2mm end mill. Subsequently, a 1.5mm slot drill was used to machine the notches. Finally, the samples were stacked before the sides were machined to ensure consistency between specimens.

To still achieve the final sample dimensions of 79.5 x 12.7 x 4.8mm as given by ASTM D3846, all vertical faces were given a 2mm offset and for the top and bottom faces, an offset of 2 to 4 extra layers was applied. This resulted in a sample size before machining of 83.5 x 16.7 x 7.2mm. The notches (1.65mm wide) were deepened accordingly. Five samples were produced for each of the four nozzle sizes in both the aligned and offset method, resulting in 40 samples in total. All samples were printed in a laboratory environment at room temperature and standard relative humidity.

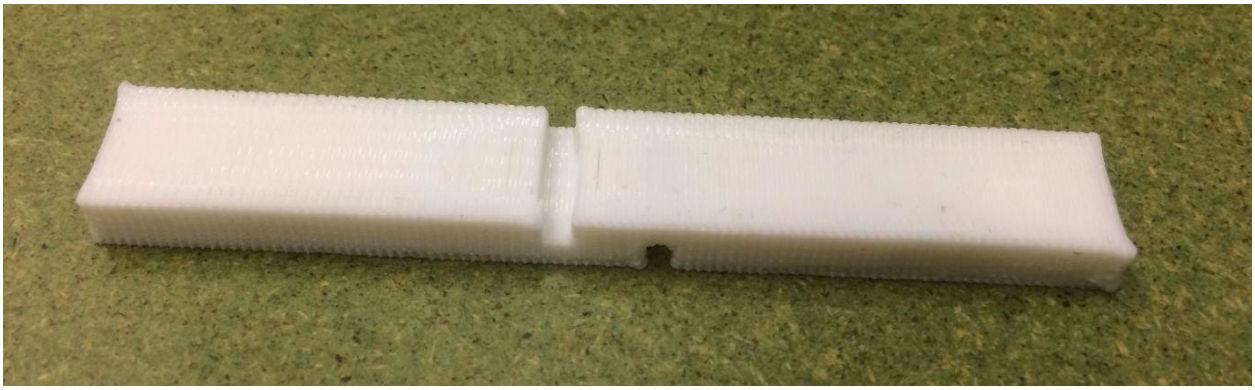

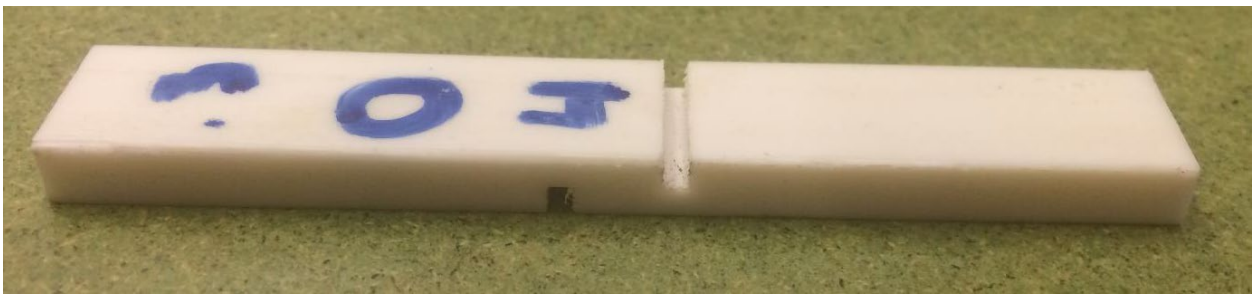

**Figure 7: The samples before (top) and after (bottom) machining [26].**

## 2.4 Void imaging sample production

To investigate the void distribution and total void area of the aligned and offset methods, the cross-section of the print, perpendicular to the road direction, needed to be exposed. Initially, methods such as hacksawing, guillotining, laser cutting, tin snipping and cold sawing were attempted. Unfortunately, these methods caused significant distortion to the roads during cutting. Secondly, a notch was machined in samples to form a stress concentration before snapping samples by hand. This led to the material exhibiting ductile behaviour and delamination between the layers. The effects were more prominent in samples with a lower nozzle size; however, the effects were found to be reduced by cooling the samples in a standard household freezer before snapping. Despite attempts to completely remove the effects, the microscopic imaging showed that there were still some indications of distortion due to the fracture procedure. The samples were tensile tested to produce a better fracture surface; however, samples experienced elongation before failure, which distorted sample cross-sections. Finally, the specimen was prepared with a double notch to form a stress concentration that lead to negligible elongation and a smooth fracture surface with minimal distortion. This approach was thus adopted to produce the sectioned samples for microscopic investigation. A nozzle size of 0.6mm was used to create the microscopic imaging sample. Then an average void area to total area ratio was calculated.

## 2.5 Experimental setup and data analysis

### 2.5.1 Shear measurements

An Instron E10000 tensile test machine was utilised to compress the samples at a rate of 1mm/min while recording the displacement of the platen and force required to do so. The sample support jig, machined as per Figure 6, is shown in Figure 8. Five samples produced through the offset method and five samples printed using the aligned method were tested per nozzle size of 0.3mm, 0.9mm, 1.2mm and 1.5mm. A total of 40 samples were thus tested. Each sample was loaded in the support jig, the bolts torqued to 0.1 Nm (±6%) in accordance with ASTM D695 [25], and the mounted sample placed in the Instron test machine to test as shown in Figure 9.

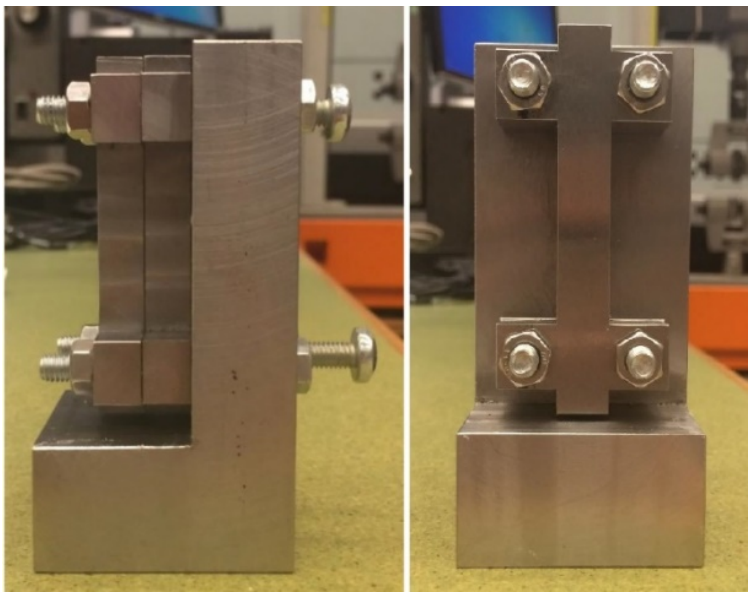

**Figure 8: The modified D695 shear jig [26].**

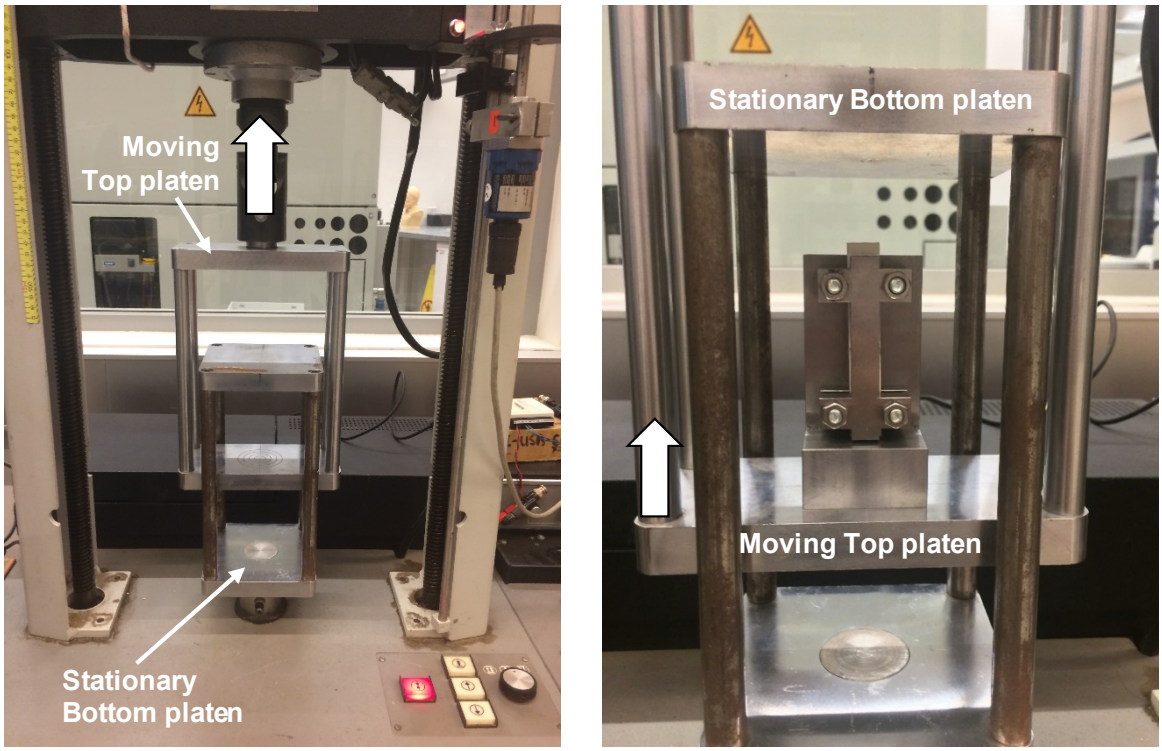


**Figure 9: Compression test setup (Instron E10000 tensile test machine) where the displacement direction of the moving top platen is indicated by the large arrow**

The measured force and displacement of the test machine's top platen for each sample is converted into a shear stress-strain graph. The measured force is converted into a stress value by dividing it by the available shear surface area of the sample, 12.7mm x 6.4mmm, as visible in Figure 6. As it is known that voids will be present in the material, the resulting stress is an average value which includes the voids along the shear surface. Such a stress value is referred to as the 'fictious' stress, as utilised by Ahmed & Susmel [16]. The force-displacement measurements are thus converted into fictitious shear stress versus strain graphs. From these graphs, the fictious shear strength and fictitious shear modulus are derived. The strain at the fictitious shear strength is also recorded. The final values of these variables are an average over five test samples. The deviation from these average values was also calculated.

### 2.5.2 Density measurements

As all samples shear at the same location and no material is lost, the weight of one side of a sheared test sample was compared to the weight of a fully dense body of the same volume. The weight of the latter (2.492g) was calculated by multiplying the body volume (2373 $mm^3$) of the sheared test sample by the OEM supplied density of fully dense ABS feedstock (1.05g/$cm^3$). The weights of all samples are converted into densities via the same approach and the final density per nozzle size is the average of five samples. The deviation from this average was also calculated.

### 2.5.3 Void area measurements

The two halves of each sample were clamped vertically to expose their cut faces under an Olympus OLS5000 3D laser scanning confocal microscope. The most undistorted portion of the cross-section was scanned. The commercial software Solidworks was employed to automatically trace the outline of each void in the microscopic images. The total void area in the scan area were obtained by summing the area of each individual void.

## 3 Experimental results and discussion

### 3.1 Shear stress-strain

The measured force-displacement graphs have been converted into fictious shear stress versus strain graphs for all samples, some of which are shown in Figure 10. The differences in the curves are attributed to small differences in printing parameters, such as inevitable temperature and humidity fluctuation, next to common differences during experimental testing such as small variation in jig-sample friction values. The region at the start of the graph represents a settling of the sample under compression, as per ASTM D695 [25], and this so called ‘toe region’ is to be excluded as it does not represent a material property. An example of such a toe region is indicated by line AC in Figure 11. The linear behaviour of the material is then captured by fitting line CD to the linear portion of the graph. This linear approximation originates at point B, which is then defined as the new zero-strain point from which any strain values are to be measured. This method is applied to all fictitious shear stress versus strain graphs and two examples of such an approximation are shown in Figure 10, labelled ‘0.3 Aligned 1_Linear’ and ‘1.2 Offset 5_Linear’.

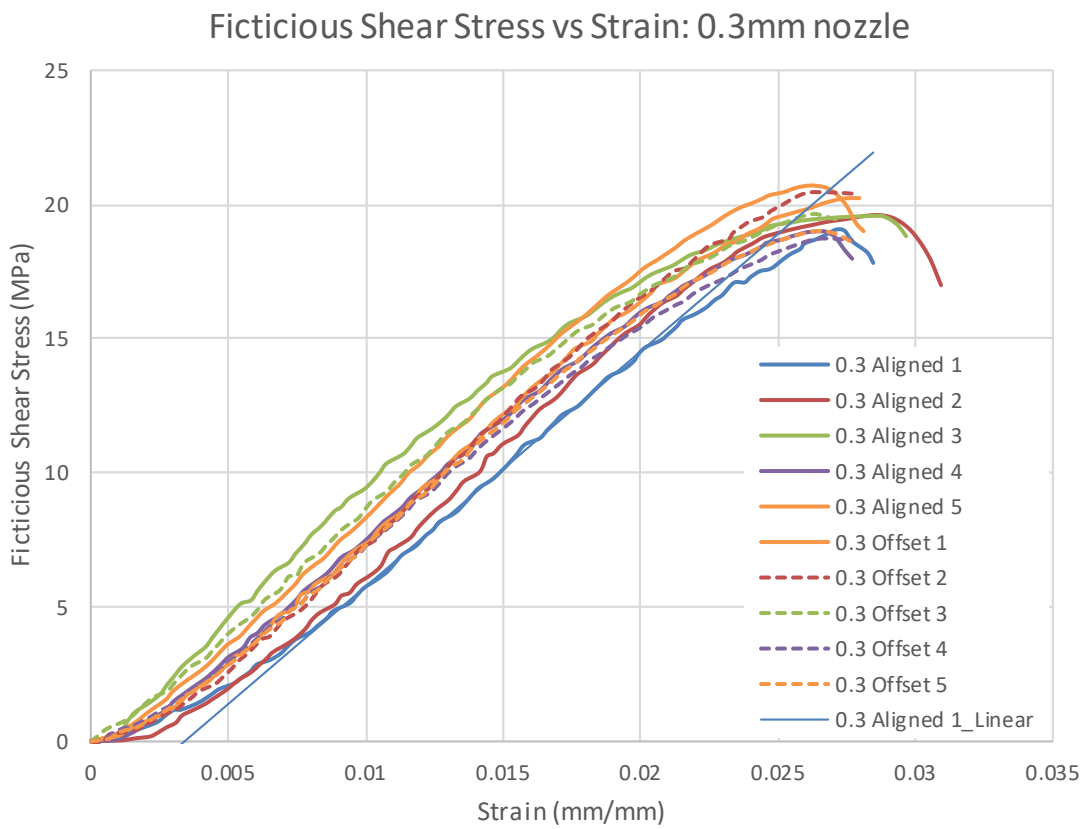


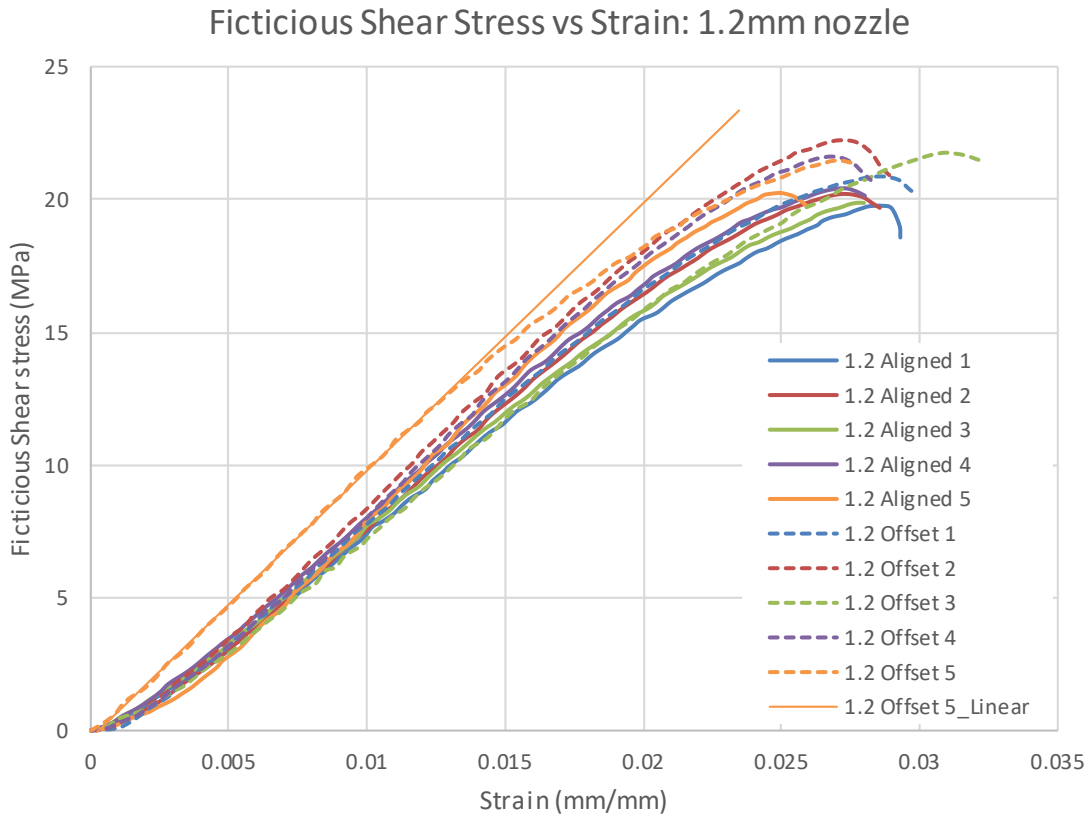


**Figure 10: Fictitious Shear Stress versus Strain graphs of the tested samples of the offset method and the aligned method at a nozzle size of 0.3mm and 1.2mm.**

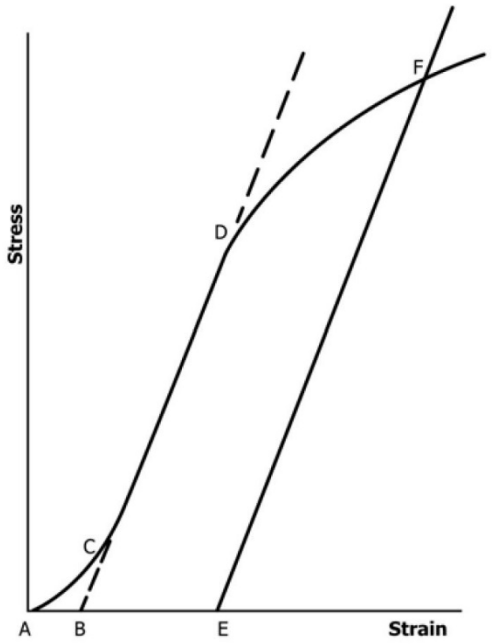


**Figure 11: Toe compensation for material with Hookean (linear) behaviour [25].**

All samples indeed show a portion of linear-elastic shear behaviour, after which a nonlinear plastic deformation stage is visible until the highest fictitious shear stress of the material, the fictitious shear strength, is reached. Rapid failure follows after this point. The value of the fictitious shear strength as the nozzle size is increased is plotted in Figure 12 and the strain value accompanying this point is plotted in Figure 13, compensated for the new zero strain point. The fictitious shear modulus, the gradient of the linear portion of each graph, is plotted in Figure 14 as the nozzle size is increased.

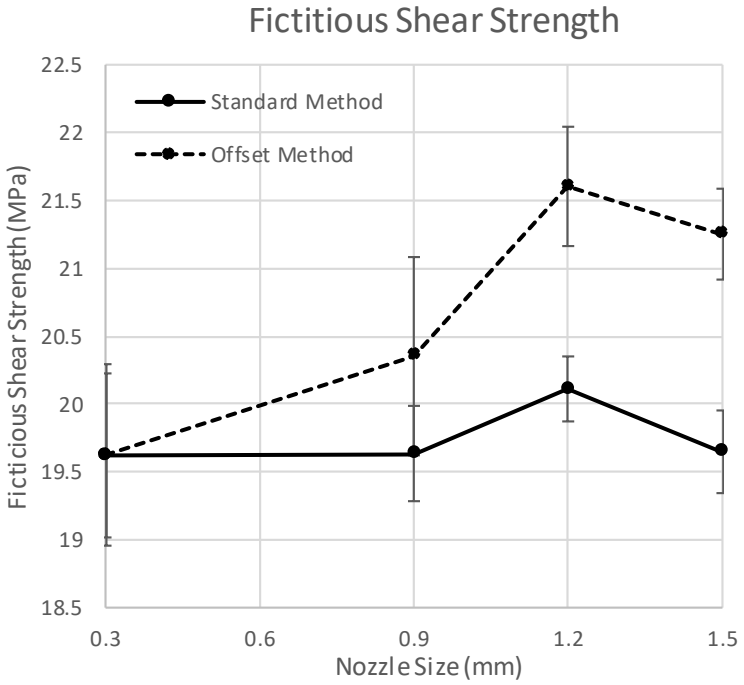


**Figure 12: Fictitious Shear Strength versus nozzle size comparison of the two FFF methods.**

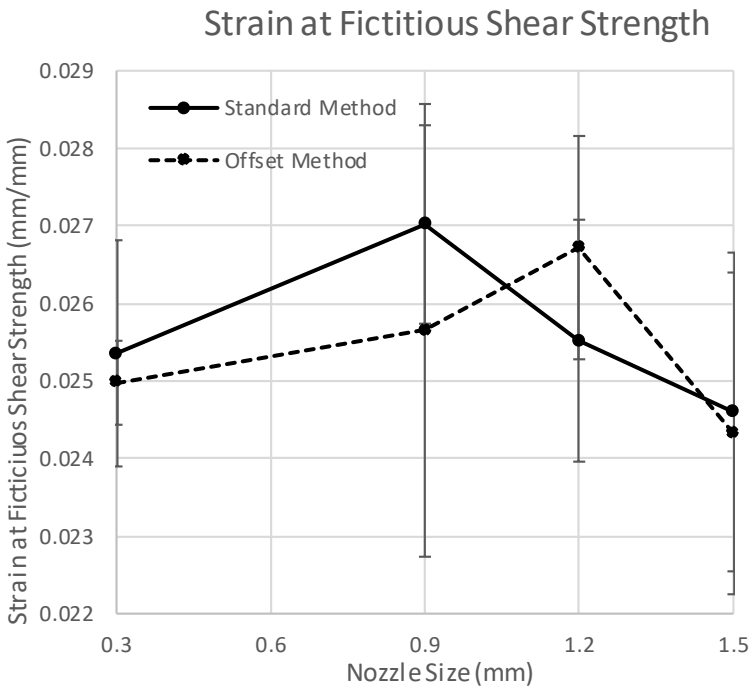


**Figure 13: Strain at the fictitious shear strength versus nozzle size comparison of the two FFF methods.**

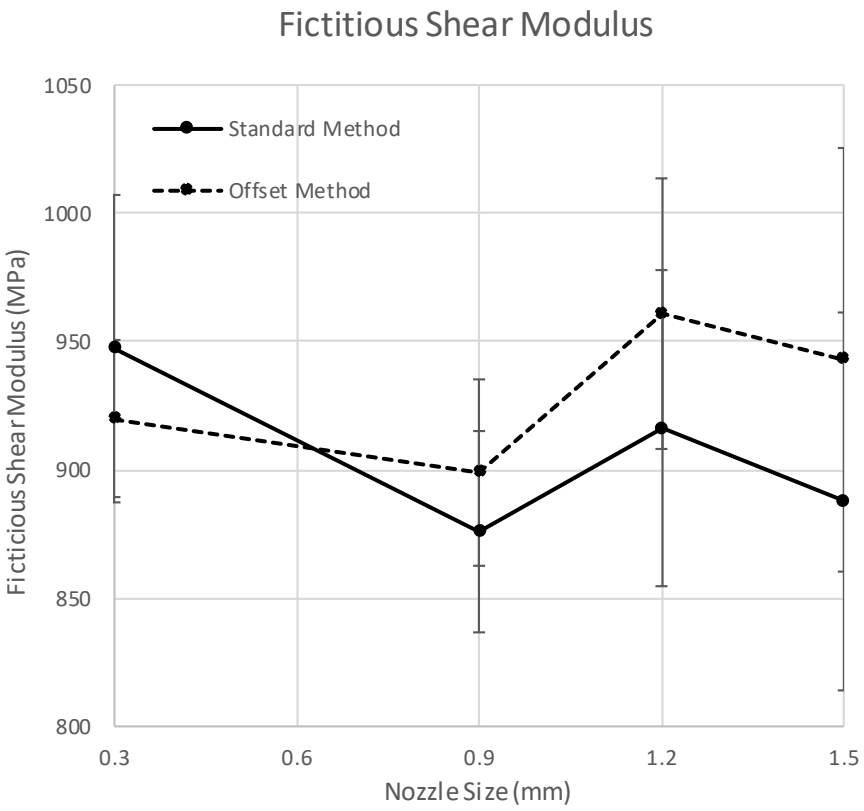


**Figure 14: Fictitious Shear Modulus versus nozzle size comparison of the two FFF methods.**

Figure 12 shows that the aligned method of FFF exhibits a nearly constant or slowly increasing shear strength as nozzles sizes increase. On the other hand, the shear strength of the offset method is shown to improve as the size of the nozzles increase. The improvement in shear strength of the offset method over that of the aligned FFF technique is shown in Figure 15.

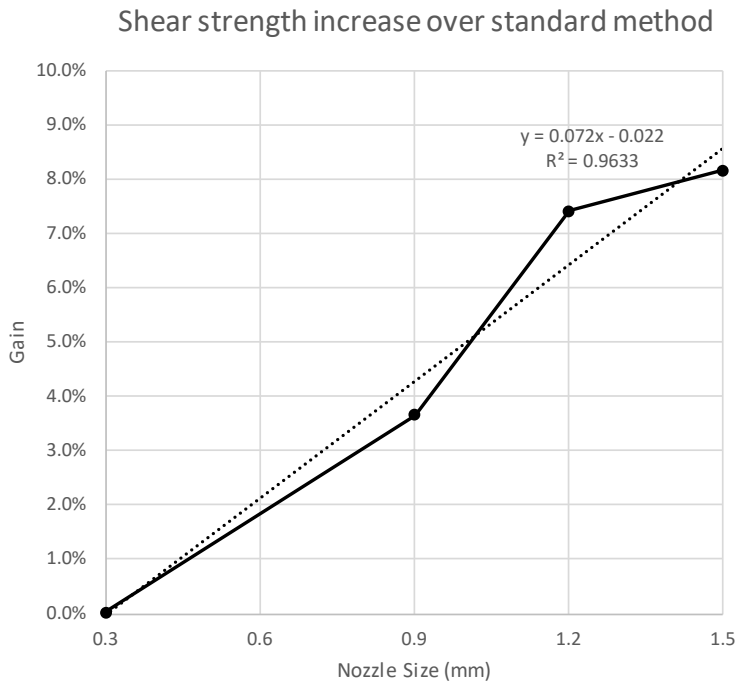


**Figure 15: Fictitious shear strength gains of the offset method over the aligned method.**

With regards to shear strength, it can be stated that the offset method has a continuous and increasing improvement over the aligned method with regards to shear strength as the nozzle size increases. The improvement in shear strength of the offset method over the aligned method is best approximated by a linear trendline ($R^2$ value of 0.96) which delivers a 7.2% shear strength improvement per millimetre increase in nozzle size.

Figure 13 indicates that no real change of the strain values at which these fictitious shear strengths are reached are visible, nor does there seem to be a dependency on the nozzle size when the margins of error are taken into account.

The fictitious shear modulus of Figure 14 seems to depict a slowly increasing modulus for the offset method compared to a decreasing modulus for the aligned method. The measurements thus indicate that the offset method produces an increasingly stiffer material when printed with increasingly larger nozzle sizes compared to the aligned method. This topic is further investigated via FEM analyses in section 3.4.

## 3.2 Density

The resulting average density values for the different nozzle sizes are shown in Figure 16, including the deviation from the average (horizontal bars).

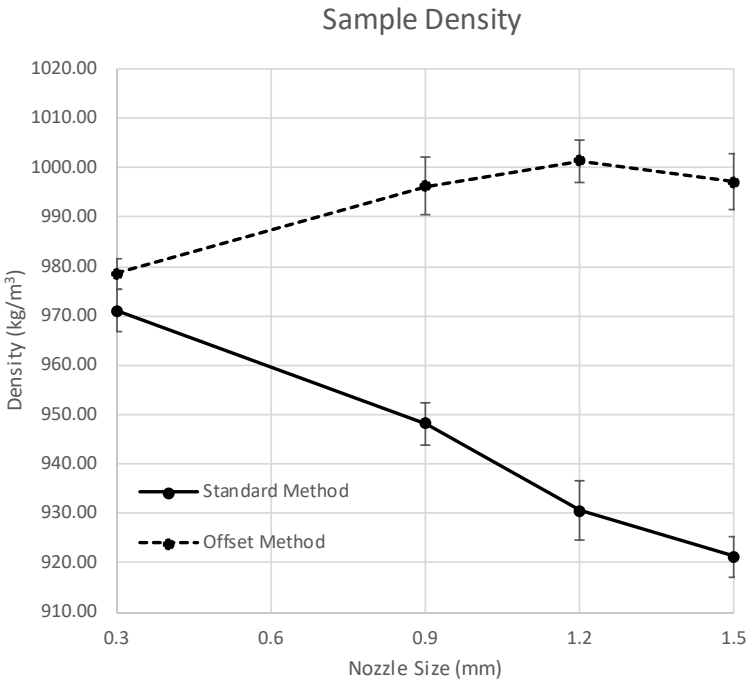


**Figure 16: Density versus nozzle size comparison of the two methods.**

This data demonstrates that samples produced through the aligned method of FFF decrease in density with an increase in nozzle size. As the volume of the samples is constant, it can be concluded that the void volume, and thus the porosity, of the sample is increasing. A very different effect can be seen when the sample is printed via the offset FFF method. Figure 16 shows that the sample density initially increases with nozzle size and then levels out at a density of roughly 1000 kg/m³. The improvement in density of the offset method over the aligned method is shown in Figure 17.

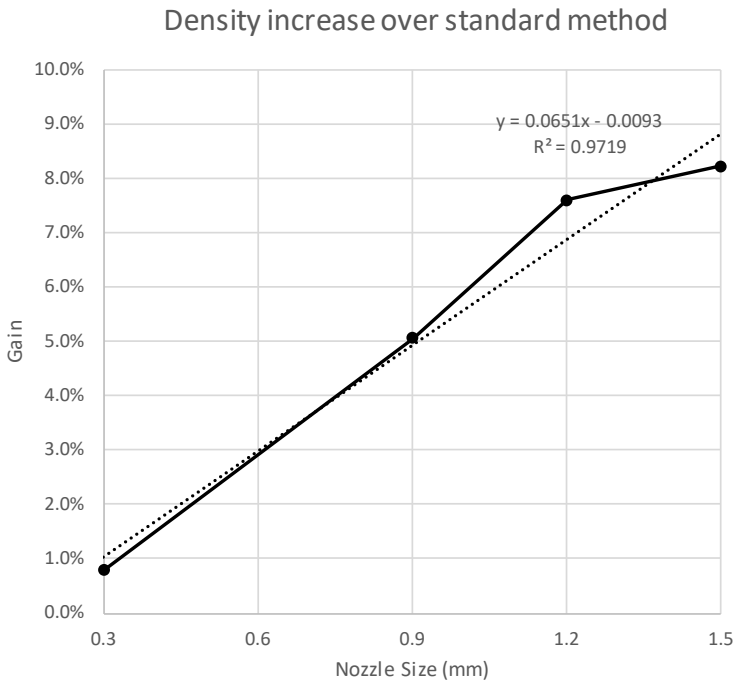


**Figure 17: Density gains of the offset method over the aligned method.**

With regards to density; the offset method shows a continuous and increasing density improvement over the aligned printing method as the nozzle size is increased. The improvement in density of the offset method over the aligned methods is best approximated by a linear trendline ($R^2$ value of 0.97), which delivers a 6.5% density improvement per millimetre increase in nozzle size increase.

### 3.3 Void analysis and unit cell creation

The microscopic images of a sample printed through the offset method and one printed through the aligned method using a 0.6mm print nozzle are shown in Figure 18. The equivalent when using a 1.2mm print nozzle is shown in Figure 19. The aligned method is on the left and the offset method is on the right in each figure.

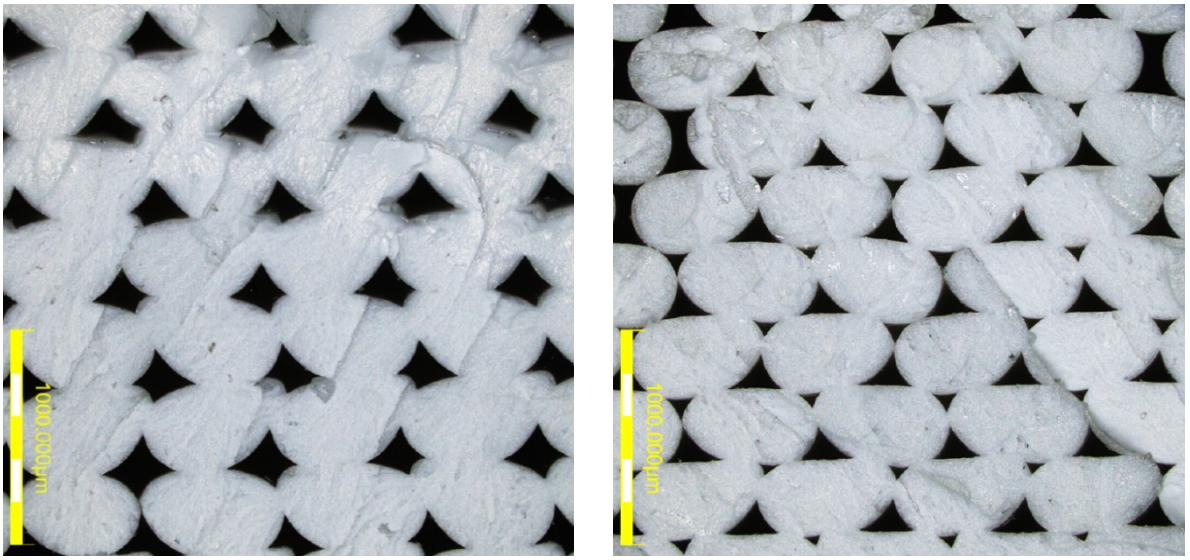


**Figure 18: Cross section of samples fabricated using the aligned (left) and offset method (right) for the 0.6mm nozzle size.**

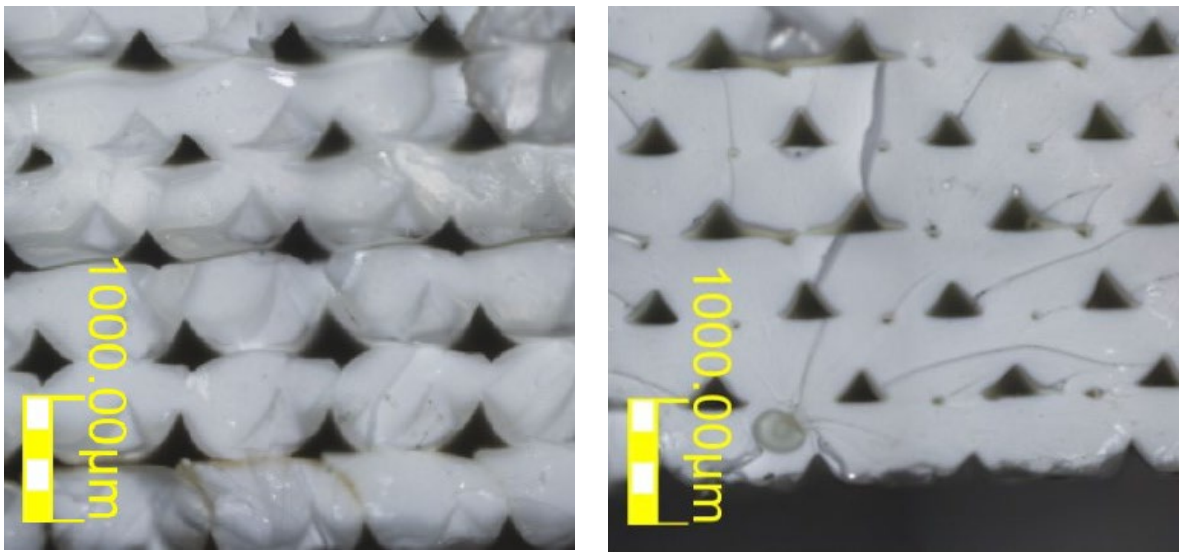


**Figure 19: Cross section of samples fabricated using the aligned (left) and offset method (right) for the 1.2mm nozzle size.**

Inspection of Figure 18 and Figure 19 reveal different features in the offset and aligned methods. The different stacking of the roads in the two methods is clearly visible, as is the reduced height per unit road cell (refer Figure 5) of the offset method. In both aligned samples, the voids are diamond shaped which is in rough agreement with the theoretical unit cell shown in Figure 4. The

images show, however, that the top of each road is flatter compared to the theorical model. It's likely that the bottom of the road solidifies quickly when deposited, thus retaining its curved shape, while the tensile forces induced by the moving nozzle result in a flattening of the top surface of the road. This results in the bottom of the diamond shaped voids to be blunter than the top. Both samples produced through the offset method shows a similar effect, a rounded bottom of the road combined with a flat top. The resulting effect on the voids in the offset method is a triangular larger void, further referred to as the 'central void', flanked by a smaller inversed triangular void. The shape of these voids in the aligned method does not markedly change but the offset method shows a different void pattern as the nozzle size is increased. The central void in the offset method maintains a similar shape but the flanking void is clearly smaller relative to the roads for a print with a larger nozzle size.

To quantify this effect, the cross-section profiles of the four samples in Figure 18 and Figure 19 were digitised to allow measurements of the values shown in Figure 20. The average value and standard deviation of these road variables are listed in Table 3 for all four samples.

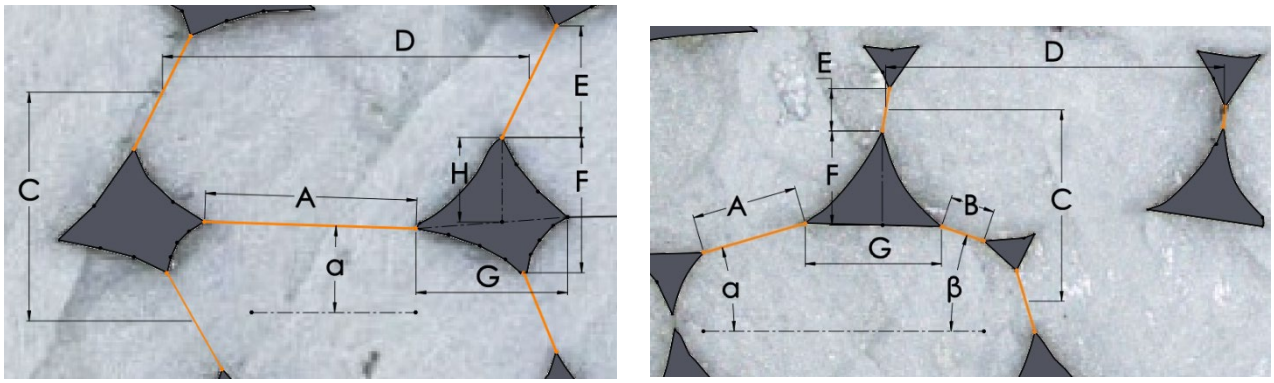


**Figure 20: Road variables of the aligned (left) and offset method (right).**

| Road variables | Sample | | | |
|---|---|---|---|---|
| | 0.6mm Aligned | 0.6mm Offset | 1.2mm Aligned | 1.2mm Offset |
| **Contact Length A (std. dev)** | 328.2µm (37.8) | 138.5µm (42.3) | 735.3µm (70.2) | 413.1µm (51.0) |
| **Contact Length B (std. dev)** | - | 138.0µm (44.8) | - | 386.3µm (73.7) |
| **Contact Angle α (std. dev)** | 2.82deg (2.44) | 16.14deg (5.67) | 0.44deg (3.94) | 7.45deg (4.12) |
| **Contact Angle β (std. dev)** | - | 15.51deg (5.67) | - | 6.61deg (2.99) |
| **Road Height C (std. dev)** | 398.6µm (15.2) | 338.0µm (13.4) | 795.3µm (26.7) | 674.2µm (2.20) |
| **Road Width D (std. dev)** | 600.6µm (25.6) | 594.5µm (17.4) | 1203.1µm (24.5) | 1201.3µm (11.1) |
| **Vertical Contact Length E (std. dev)** | 165.4µm (35.0) | 73.2µm (30.8) | 450.1µm (59.0) | 344.3µm (38.6) |
| **Central Void Height F (std. dev)** | 231.2µm (30.6) | 155.4µm (11.3) | 315.0µm (27.6) | 255.4µm (23.0) |
| **Central Void Width G (std. dev)** | 272.0µm (28.5) | 232.6µm (15.5) | 450.1µm (73.4) | 354.2µm (43.4) |
| **Central Void Bias H (std. dev)** | 156.8µm (12.9) | - | 221.3µm (38.3) | - |

| | | | | |
|---|---|---|---|---|
| **Sample area** | 6.6254e6 $\mu m^2$ | 6.6254e6 $\mu m^2$ | 2.40e7 $\mu m^2$ | 1.60e7 $\mu m^2$ |
| **Void surface area** | 11.94% | 10.17% | 8.12% | 5.77% |
| **Reduction in void surface area over the 0.6mm sample** | | | 3.83% | 4.40% |

**Table 3: Average values of the road variables for the samples printed with the offset and aligned method in 0.6mm and 1.2mm nozzle sizes.**

Various aspects can be derived from the results in Table 3 and are described below.

Firstly, the data in Table 3 allows an update of the theoretical unit cell, given in Figure 5, to reflect a realistic unit cell of a sample produced via the offset and aligned method using a 0.6mm and 1.2mm nozzle. Such realistic unit cells are shown in Figure 21, where the 0.6mm unit cells are enlarged twice and overlaid onto the 1.2mm unit cells to allow a straightforward visual comparison.

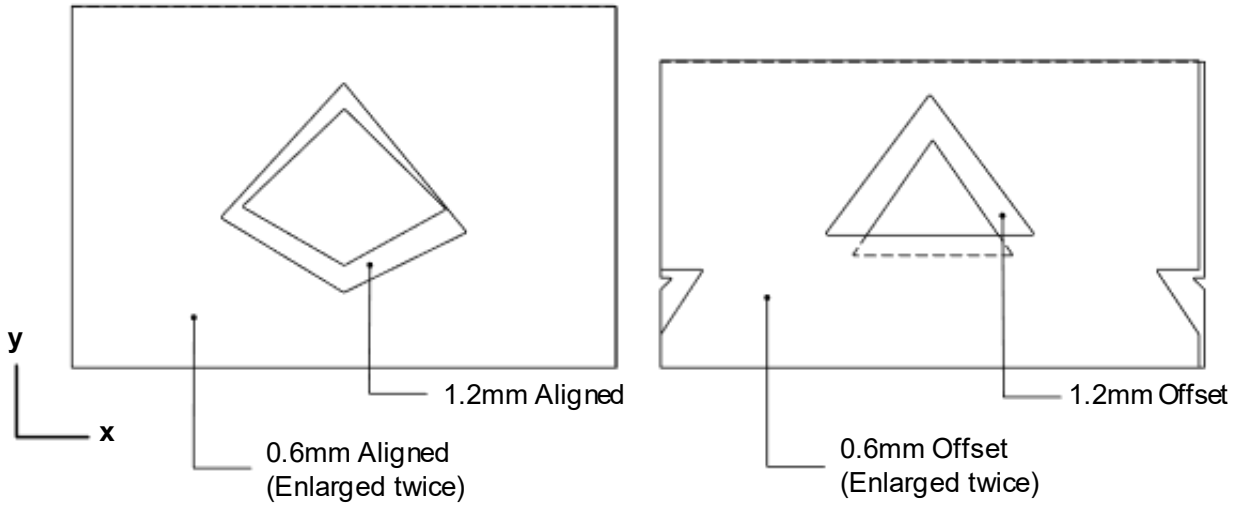


**Figure 21: The feedstock content of a realistic unit road cell for both FFF methods. The 0.6mm unit cells (in front) are enlarged twice to allow straightforward comparison with the 1.2mm unit cells (behind).**

Figure 21 clearly shows the previously noted effect; a central blunted diamond shaped void in the aligned method, and a central triangular void flanked by a smaller inversed triangular void in the offset method. The change in this flanking void when the nozzle size is increased is evident. These unit cells will be used in the FEM analyses in section 3.4.

Secondly, the results in Table 3 show that for the samples printed with the 0.6mm nozzle, the offset method has a smaller void surface area percentage (10.2%) compared to that of the aligned method (11.9%). The 1.2mm sample also has a smaller void surface area for the offset method (5.7%) compared to the aligned method (8.1%). The offset method thus produces a consistently denser material compared to the aligned method.

Thirdly, the average contact length A and B in Table 3 can be summed to create the total average interlayer contact length in a unit cell for each printing method. This total average interlayer contact length per unit cell can be converted into an average interlayer contact length over the shear surface of the sample, taken to be 6.4 x 12.7mm in Figure 6, as follows. As the roads run parallel to the 12.7mm dimension, the number of roads along the shear surface is determined by dividing the length 6.4mm (6400µm) by the average road width as found in Table 3. The total average interlayer contact length per unit cell, the number of roads in the contact area and the total contact length along the shear surface are listed Table 4.

| | Sample | | | |
|---|---|---|---|---|
| | **0.6mm Aligned** | **0.6mm Offset** | **1.2mm Aligned** | **1.2mm Offset** |
| **Average total contact length per unit cell** | 328.2μm | 276.5μm | 735.3μm | 799.3μm |
| **Number of roads along the shear surface** | 10.66 | 10.77 | 5.32 | 5.33 |
| **Total contact length along the shear surface** | 3497.4μm | 2977.0μm | 3911.8μm | 4258.5μm |
| **Increase of the total contact length over the 0.6mm sample** | | | 11.85% | 43.05% |

**Table 4: Total contact length for the samples printed with the offset and aligned method for the 0.6mm and 1.2mm samples.**

The results in Table 4 show that the total contact length between two layers of a shear sample increases faster in the offset method compared to the aligned method.

The findings from the void analysis can be summarised as follows. The area of voids in the samples printed through the offset method decrease slightly faster than that in the samples created using the aligned method. This reduction of the area of voids, combined with a difference in void shape and placement, leads to a faster increasing interlayer contact length in the offset method compared to the aligned method. The effects of such a faster increasing contact length on the shear modulus and real shear stress were investigated using a FEM analysis.

## 4 FEM analysis

The findings from section 3 indicated that the fictitious shear modulus of offset samples showed a small increase compared to a small decrease for aligned samples. This outcome, however, is accompanied by relatively large error margins. This section will utilise the Finite Element Method (FEM) to analyse the unit cells of Figure 21 to determine the real shear stress values in detail and assess the effects of the difference in unit cells per printing method on the fictitious shear modulus.

Key settings and assumptions used in the FEM analysis of the unit cells of Figure 21 are as follows.

The material properties used to compare the offset printing to the aligned printing method on a microstructural scale should reflect those of the feedstock material. As the FEM analyses are aimed towards investigating the difference in shear response of the offset relative to the aligned method, the tensile stress-strain graph for the feedstock ABS as found by Casavola et al. [4] can be used to assess this relative behaviour. The stress-strain curve of the feedstock material, labelled ‘wire’ in Figure 2, is approximated by a bilinear material model as shown in Figure 22 and applied to the FEM analyses.

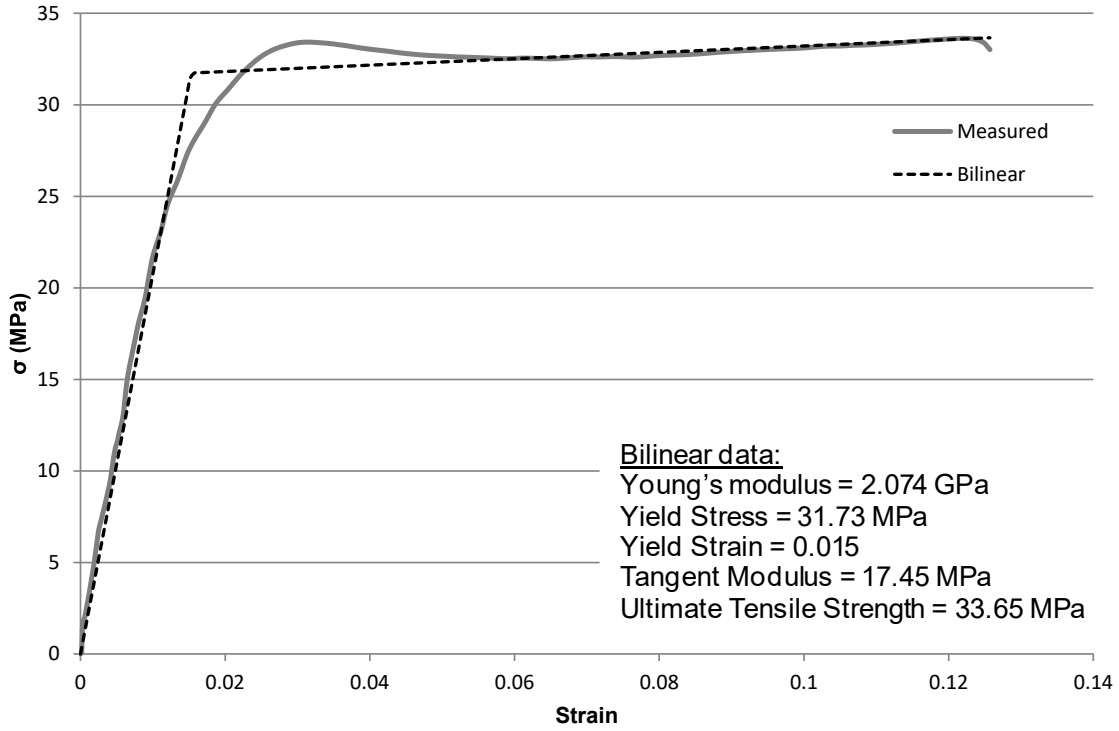


**Figure 22: The tensile stress-strain graph of feedstock ABS [4] approximated by a bilinear material model.**

The nature of the FFF prints with long uniformly parallel roads allows a 2D FEM analysis of the unit cells when a plain strain condition (no strain in the z- direction) is applied. Each unit cell is assigned a linear symmetry condition on their left and right side, which replicates neighbouring unit cells. A displacement of 0.004mm is applied to the top of each unit cell in the positive x-direction while constraining movement in the y-direction in the coordinate system shown in Figure 21. All degrees of freedom of the bottom edge are set to zero.

The unit cells are meshed with linear 2D 4-node Plane182 elements with a general size of 0.005mm. Each corner of the voids is rounded to a radius of 0.002m to eliminate infinitely high stresses at an infinitely sharp corner. A curvature mesh refinement was applied to these rounded corners by ensuring each mesh element only spans 2°. An inflation layer mesh refinement is subsequently applied to the circumference of each void to ensure the first elements adjacent to each void have a size of 0.0001mm. The resulting mesh for the 1.2mm unit cell is shown in Figure 23.

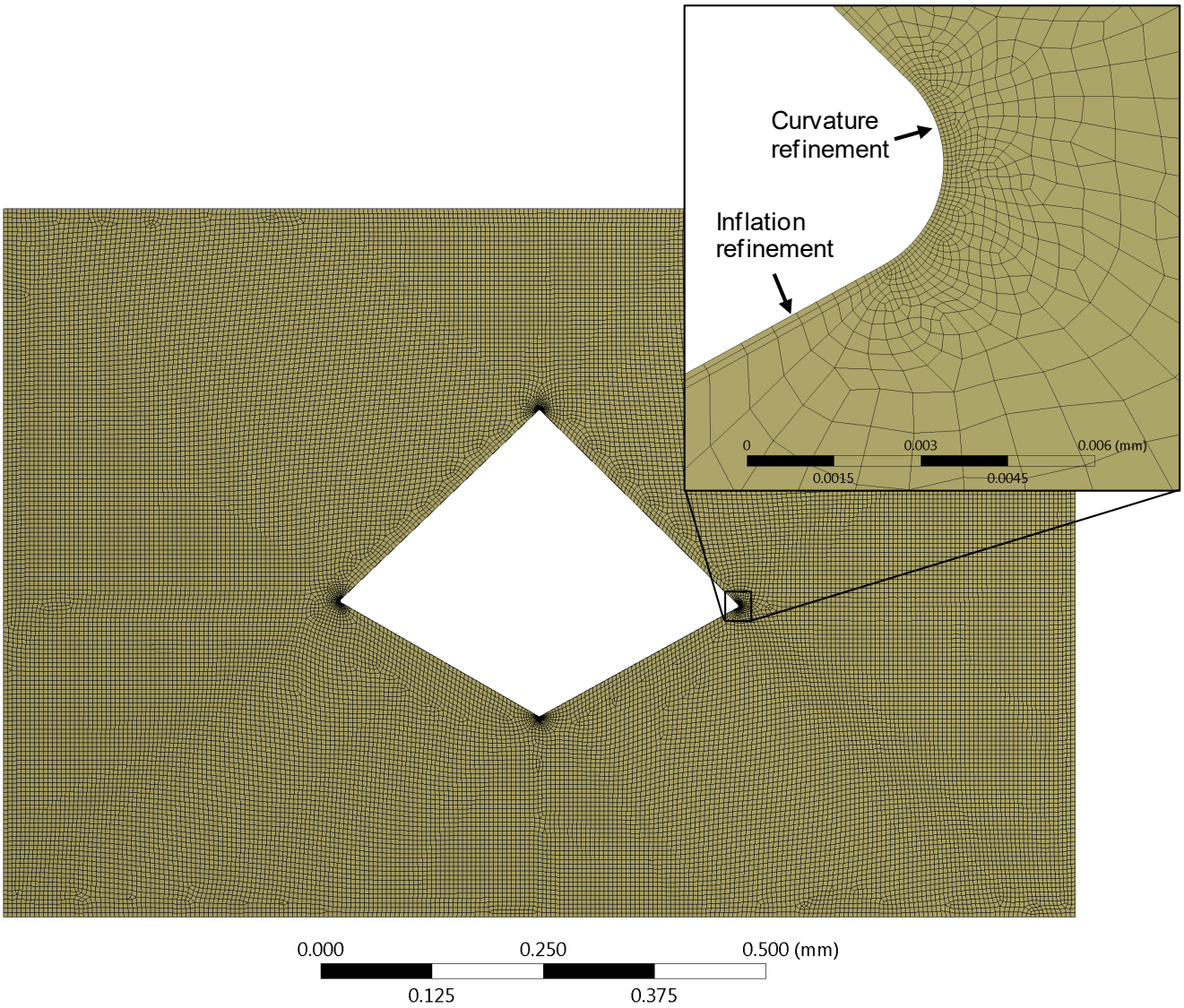


**Figure 23: The mesh of the 1.2mm unit cell with a close-up indicating the mesh refinements.**

The real shear stress distribution, as opposed to the fictitious shear stress, for all four samples are shown in Figure 24 and Figure 25. An extra purple band is added to the legend, which lower value is set to 13 MPa for the 0.6mm samples and 6 MPa for the 1.2mm samples, to allow better visualisation of the stress distribution away from the highly localised stress maxima.

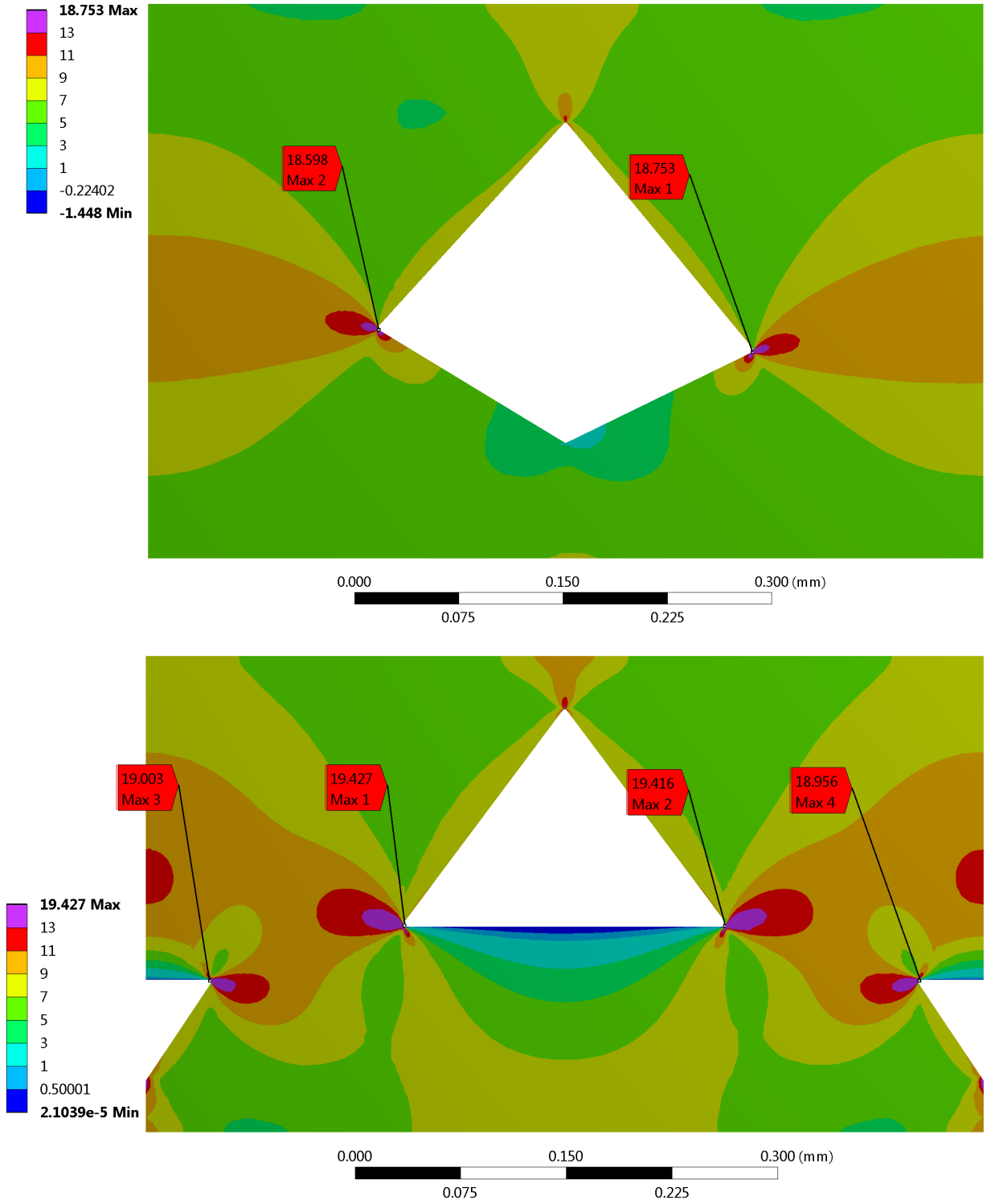


**Figure 24: The shear stress of the aligned method (Top) and the offset method (Bottom) for the 0.6mm unit cell.**

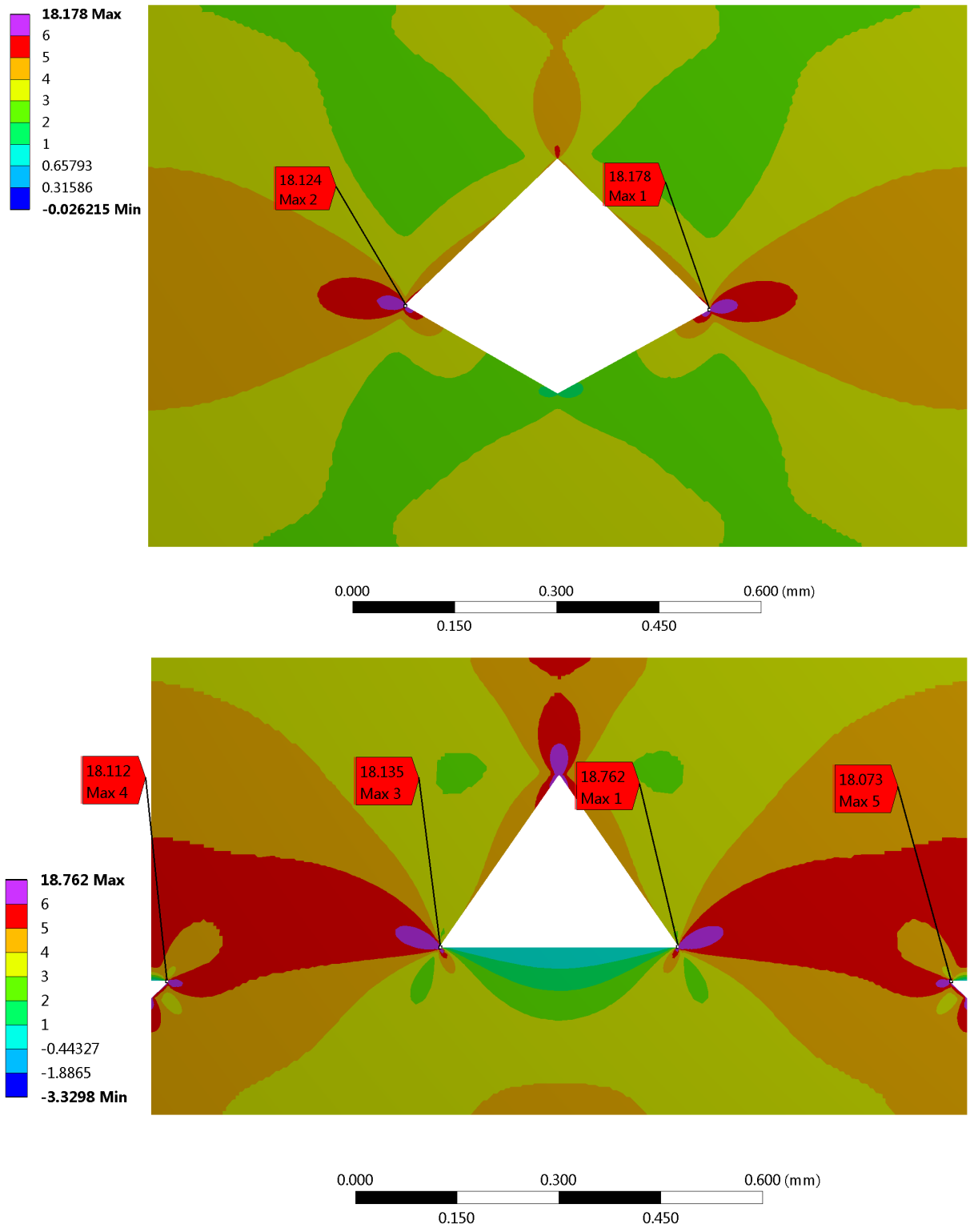


**Figure 25: The shear stress of the aligned method (Top) and the offset method (Bottom) for the 1.2mm unit cell.**

As expected, the highest shear stress is found at the corners of the voids in each unit cell. The development of the real shear stress at these points of maximum stress is of interest and the FEM analysis was thus set to ramp the applied displacement to its maximum value of 0.004mm over 100 sub steps. This allows the stress development to be plotted against an increasing displacement value, as shown in Figure 26.


**Figure 26: The development of the maximum shear stress of the offset method and the aligned method as the displacement increased in 30 sub steps to a value of 0.004mm.**

The highest stress values shown in Figure 24 and Figure 25 show similar real shear stress values that are around 18 to 19 MPa as listed in Table 5. Figure 26 clarifies these findings as the notable kink in the graphs and indicates that all unit cells are experiencing plastic deformation. Due to the low tangent modulus of the material, the real shear stress maxima differ very little in value.

| | Sample | | | |
|---|---|---|---|---|
| | **0.6mm Aligned** | **0.6mm Offset** | **1.2mm Aligned** | **1.2mm Offset** |
| **Maximum Shear stress** | 18.573 MPa | 19.247 MPa | 18.178 MPa | 18.762 MPa |
| **Shear stress decrease over the 0.6mm sample** | | | 2.13% | 2.52% |

**Table 5: Shear stress of the unit cells.**

In addition to the stress development of points of maximum stress, the shear stress along the line of contact between roads is of interest. These contact lines, as shown in Figure 27 for the 1.2mm unit cells, are set to connect the points of maximum stress of each unit cell as found in Figure 24 and Figure 25. The coordinate systems used per line are shown in Figure 27 and the real shear stress measurements per line are shown in Figure 28 and Figure 29.

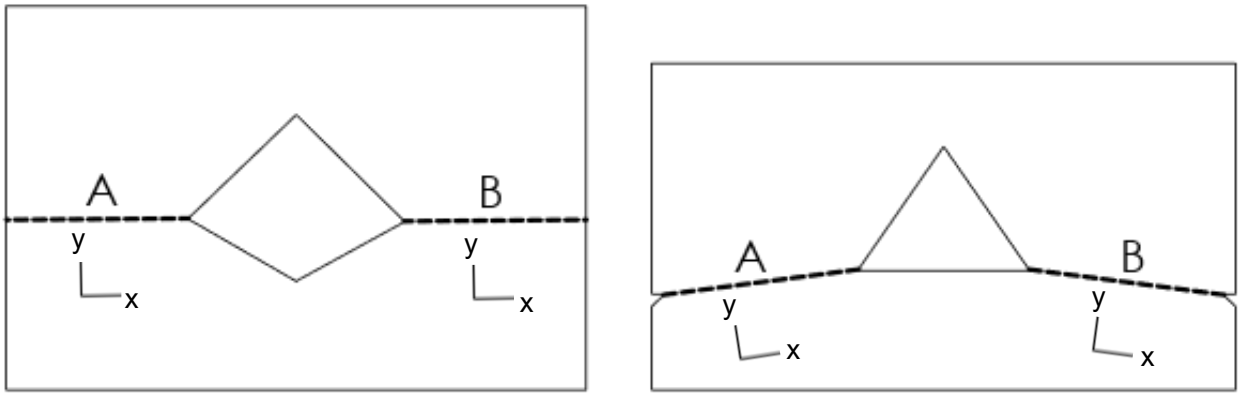


**Figure 27: The shear lines of the 1.2mm unit cell for the aligned (left) and the offset (right) printing method including the coordinate systems per contact line.**

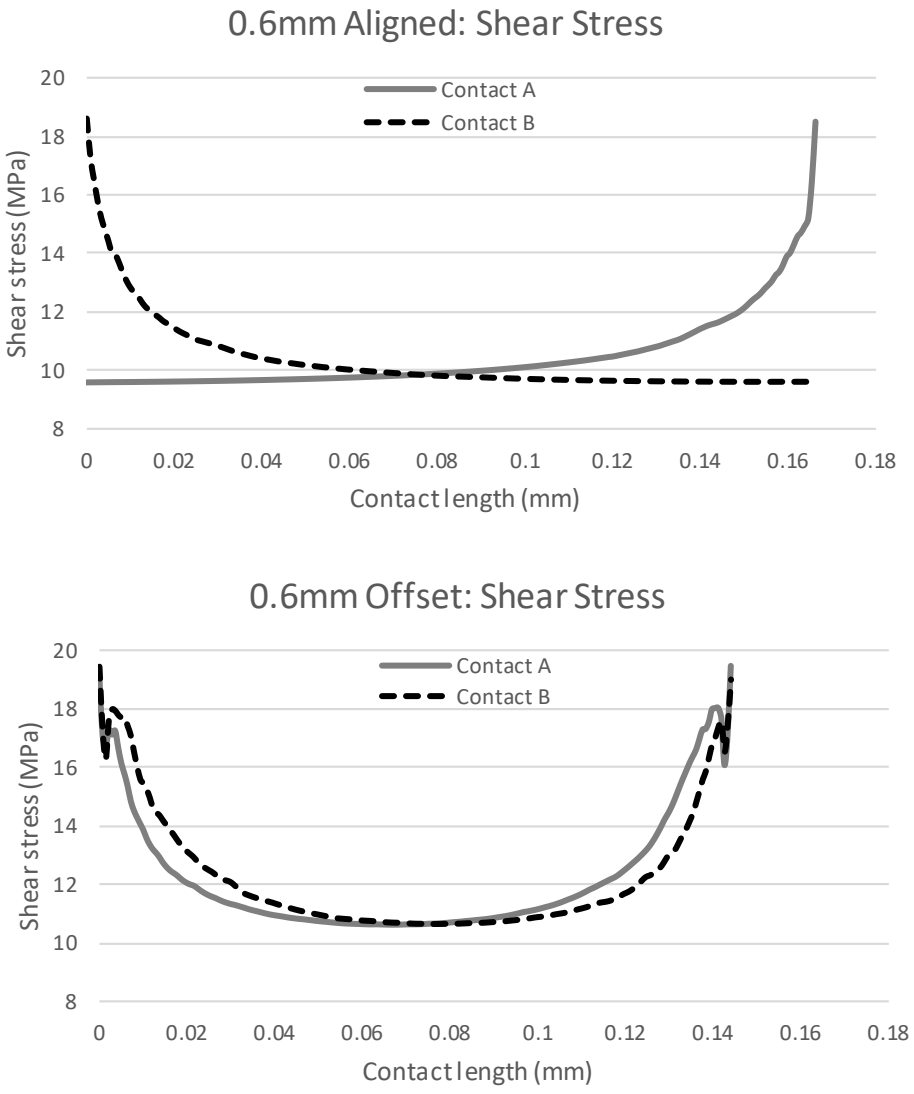


**Figure 28: The shear stress of the aligned method (Top) and the offset method (Bottom) along a line connecting the points of maximum stress of the voids for the 0.6mm unit cell.**

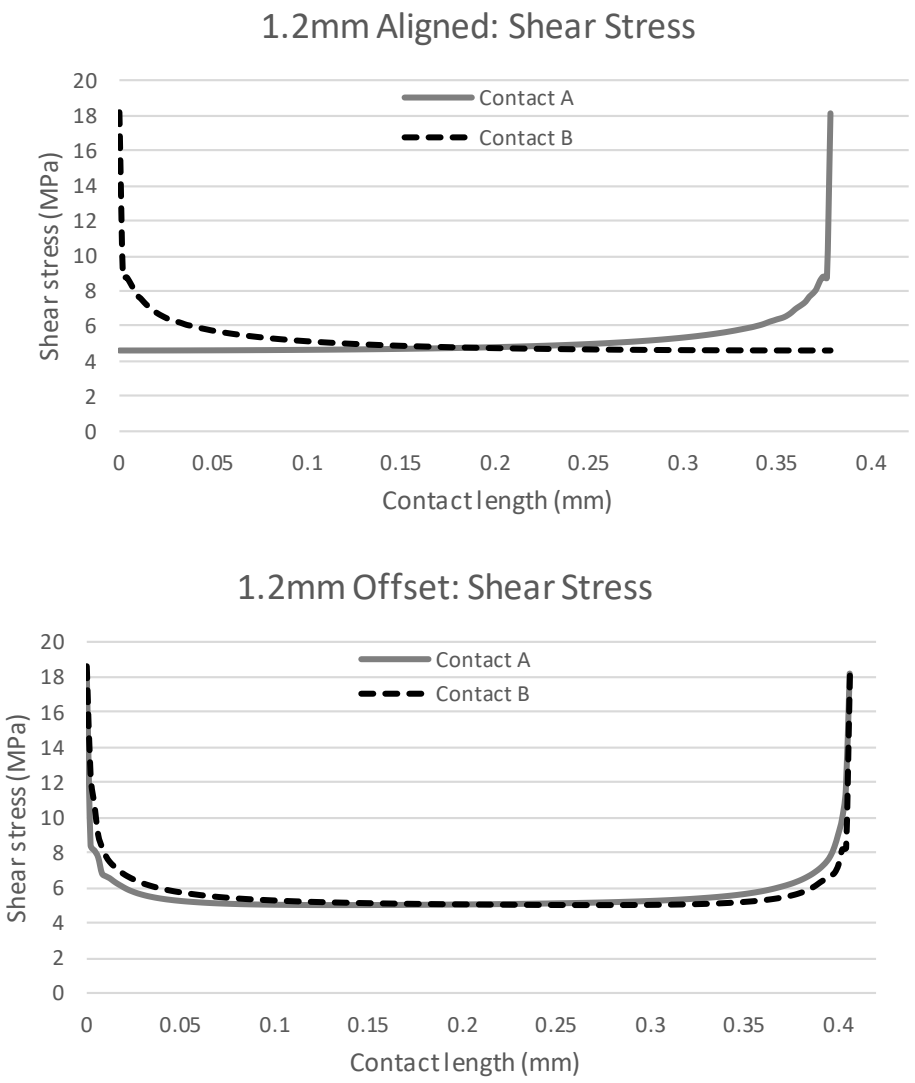


**Figure 29: The shear stress of the aligned method (Top) and the offset method (Bottom) along a line connecting the points of maximum stress of the voids for the 1.2mm unit cell.**

The metric used to compare the results from Figure 28 and Figure 29 is the well-known 'Stress Concentration Factor ($K_{tn}$)', commonly used to compare the impact of holes of different geometry in the stress state of plates, being defined by Pilkey [27] for shear stress as:

$$K_{tn} = \frac{\tau_{max}}{\tau_{ave}}$$

Where $\tau_{max}$ is the maximum, and $\tau_{ave}$ the average shear stress values from Figure 28 and Figure 29. The results averaged over the two contact areas for all unit cells are given in Table 6.

| | Sample | | | |
|---|---|---|---|---|
| | **0.6mm Aligned** | **0.6mm Offset** | **1.2mm Aligned** | **1.2mm Offset** |
| **Maximum shear stress (MPa)** | 18.55 | 19.45 | 18.14 | 18.40 |
| **Average shear stress (MPa)** | 10.42 | 12.28 | 5.15 | 5.60 |
| **Stress Concentration Factor $K_{tn}$** | 1.78 | 1.58 | 3.52 | 3.28 |
| **$K_{tn}$ increase over the 0.6mm sample** | | | 222.2% | 207.2% |

**Table 6: Stress Concentration Factor $K_{tn}$ of the unit cells.**

Table 6 shows that the offset printing method produces a structure with lower stress concentration factors than a structure created through the aligned method. Additionally, the increase in stress concentration factor, as the nozzle size is increased, is slower for the offset method compared to the aligned method.

The fictitious shear modulus, as discussed earlier, is also assessed per unit cell by creating a fictitious shear stress versus strain graph from the FEM results. The force needed to apply the 0.004m displacement is extracted from each unit cell and converted into a fictitious shear stress by dividing it by the width of each cell times a factor of 1 to account for the plane strain approach. The displacement is converted to a strain by dividing the displacement per step by the width of the unit cells. The results are shown in Figure 30.

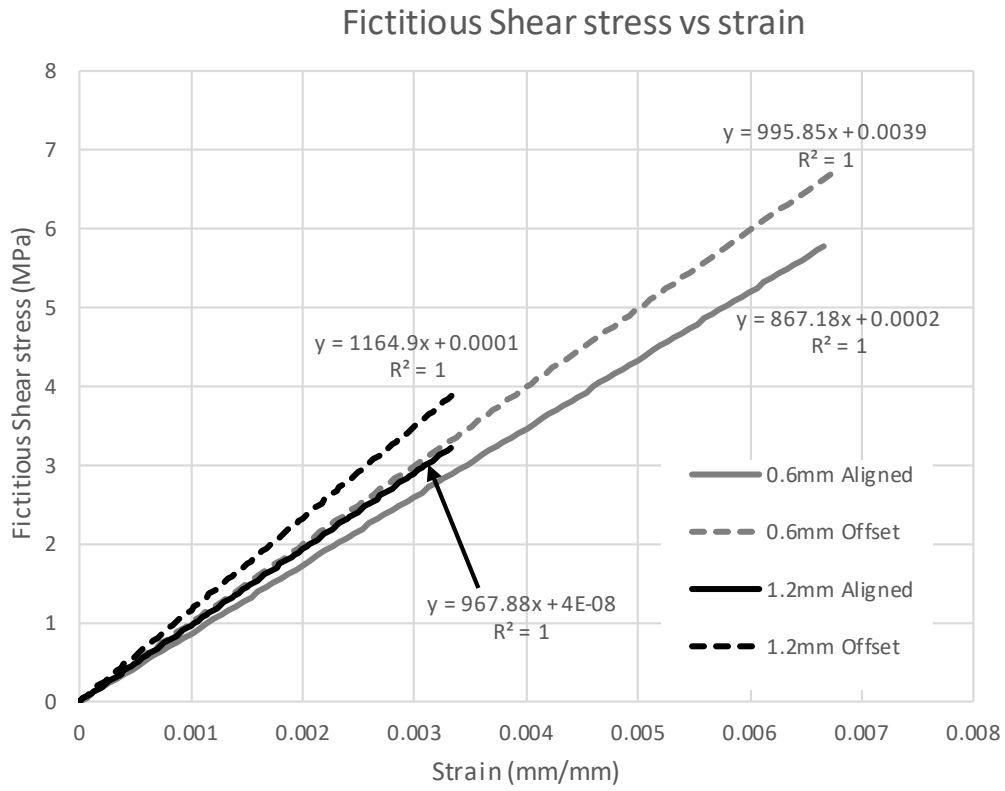


**Figure 30: The shear stress versus strain graphs of each unit cell.**

Figure 30 reveals the following aspects. As the same 0.004m displacement is applied to the 0.6mm and 1.2mm unit cells, the resulting strain of the 1.2mm samples is less due to their larger width. As such, the lines terminate earlier for the 1.2mm samples compared to the 0.6mm samples. Furthermore, the effect of the points of maximum stress on the overall shear stress behaviour of the samples is neglectable as apparent by the linear nature of the graphs ($R^2$=1). This effect is due to the low tangent modulus of the feedstock material and the subsequent low contribution to the stress value in the material after yield is reached. Finally, the shear modulus of the unit cells can be derived from the trendlines of Figure 30 and are listed in Table 7.

| | Sample | | | |
|---|---|---|---|---|
| | **0.6mm Aligned** | **0.6mm Offset** | **1.2mm Aligned** | **1.2mm Offset** |
| **Shear modulus** | 867.2 MPa | 995.9 MPa | 967.9 MPa | 1164.9 MPa |
| **Shear modulus increase over the 0.6mm sample** | | | 11.6% | 17.1% |

**Table 7: Shear modulus of the unit cells.**

The fictitious shear results from the unit cell indicate that the samples created through the offset method have a larger fictitious shear modulus than the samples printed through the aligned method. Additionally, the increase in nozzle size results in a faster increase in fictitious shear modulus of the offset printing method than that of the aligned method.

Further investigation into the offset method is envisioned. The independency of the strain values at which material failure starts is surprising in light of the higher stress concentration factors for samples produced with larger nozzle sizes. It was found that the offset method, being a stiffer material overall, introduces higher stresses and thus exhibits nonlinear material behaviour at less deformation than the aligned method. It would be reasonable to assume that the point at which material failure is initiated is also reached earlier for the offset method. A similar finding was made by Susmel & Ahmed [15] in their investigation into the static strength of notched PLA samples produced through FFF, where the sharpest notch geometry did not always result in the lowest static strength. The inclusion of fracture mechanics in FEM simulations would allow investigation of the mechanical behaviour to the point failure of the samples.

## 5 Conclusion

This paper has presented investigations into the mechanical behaviour of thin-walled structures, produced via a newly proposed 'offset' method of FFF, and compared these properties to the structures produced through the commonly used 'aligned' method of FFF production.
The results from experimental testing, microscopic image analysis and FEM simulations of both printing methods are summarised in Table 8.

| | Sample | |
|---|---|---|
| | **Offset method** | **Aligned method** |
| **Experimental: Fictitious Shear Strength** | Higher than the aligned method. Increasing with nozzle size | Lower than the offset method. Nearly independent of nozzle size |
| **Experimental: Strain at Fictitious Shear Strength** | Equivalent to aligned method. Independent of nozzle size | Equivalent to aligned method. Independent of nozzle size |
| **Experimental: Fictitious Shear Modulus** | Seemingly higher than the aligned method. Seemingly increasing with nozzle size | Seemingly lower than the aligned method. Seemingly decreasing with nozzle size |
| **Experimental: Density** | Higher than the aligned method. Increasing with nozzle size | Lower than the offset method. Decreasing with nozzle size |
| **Sample void analysis: Void surface area** | Lower than the aligned method. Slowly decreasing with nozzle size | Higher than the offset method. Slowly decreasing with nozzle size |
| **Sample void analysis: Interlayer contact length** | Lower than the aligned method for 0.6mm nozzle, higher than the aligned for 1.2mm nozzle. Quickly increasing with nozzle size | Higher than the offset method for 0.6mm nozzle, higher than the aligned for 1.2mm nozzle. Slowly increasing with nozzle size |
| **Unit cell FEM analysis: peak shear stress** | Higher than the aligned method. Small increase with nozzle size | Lower than the offset method. Small increase with nozzle size |
| **Unit cell FEM analysis: Stress Concentration Factor** | Lower than the aligned method. Large increase with nozzle size | Higher than the offset method. Large increase with nozzle size |
| **Unit cell FEM analysis: Fictitious Shear Modulus** | Higher than the aligned method. Slow increase with nozzle size | Lower than the offset method. Slow increase with nozzle size |

**Table 8: Comparison of the findings for the offset method and the aligned method**

The experimental results showed samples produced through the offset method had both an increase in density and a higher fictitious shear strength value. An investigation of the improved shear strength behaviour of the offset method and the near constant fictitious shear strength

behaviour of the aligned method was conducted via the void analysis and unit cell FEM simulations.

As the area of voids seem to decrease similarly in both printing methods as the nozzle size is increased, the difference in shape and placement of the voids between the printing methods is key. The offset method exhibits a faster increasing total interlayer contact length as the nozzle size is increased over the aligned method. This increased interconnectivity of material between layers creates an overall stiffer material, with a higher fictitious shear modulus. The aligned method indeed shows an increasing contact length and accompanying increasing fictitious shear modulus but the increase is less than that for the offset method. A material with a higher fictitious shear modulus is one aspect influencing the achievement of a high fictitious shear strength value. A second aspect affecting the fictitious shear strength is the strain at which material failure is initiated. Experimental testing found that the strain corresponding to the fictitious shear strength are equivalent between the two printing methods and not dependent on the nozzle size. As such, the material with the fastest increasing fictitious shear modulus, the offset method, will reach a higher fictitious shear strength as the nozzle size increases. The aligned method has a slower increasing fictitious shear modulus and, for an equivalent strain value, only a slow increase in fictitious shear strength is noticeable as the nozzle size is increased.

Overall, it can be stated that the offset method is a superior FFF technique for shear loaded additively manufactured parts. Adopting the offset method allows designers to increase the nozzle size, thus reduce print times, while still maintaining sufficient shear strength. Alternatively, when using the offset method designers can reduce the necessary wall thickness for a given shear load, which is beneficial when practical thin-walled structures are required.

## 6 Declaration of Competing Interest

None

## 7 Acknowledgment

The research study described herein is supported by an Australian Government Research Training Program Scholarship and is co-funded by the Department of Industry, Innovation and Science (Innovative Manufacturing CRC Ltd), the University of Technology Sydney (UTS) and Downer, via its subsidiary Mineral Technologies Pty Ltd (IMCRC/MTC/290418). The researcher would like to thank Bao Duy Ngo and Ahmad Kamal for their contributions to the findings described in this paper. In addition, the many brainstorming sessions with the UTS:Rapido and UTS:CAS team are greatly appreciated.

## References

[1] CreativeMechanisms.com, *The Effect of Layer Thickness When Using an FDM 3D Printer*, in *Creative Mechanism Blog*, C.M. Staff, Editor. 2016.

[2] Somireddy, M., A. Czekanski, and C.V. Singh, *Development of constitutive material model of 3D printed structure via FDM.* Materials Today Communications, 2018. **15**: p. 143-152.

[3] Cuan-Urquizo, E. and A. Bhaskar, *Flexural elasticity of woodpile lattice beams.* European Journal of Mechanics A/Solids, 2018. **67**: p. 187.

[4] Casavola, C., et al., *Orthotropic mechanical properties of fused deposition modelling parts described by classical laminate theory.* Materials & Design, 2016. **90**: p. 453-458.

[5] Liu, X. and V. Shapiro, *Homogenization of material properties in additively manufactured structures.* CAD Computer Aided Design, 2016. **78**: p. 71-82.

[6] Lee, B.H., J. Abdullah, and Z.A. Khan, *Optimization of rapid prototyping parameters for production of flexible ABS object.* Journal of Materials Processing Technology, 2005. **169**(1): p. 54-61.
[7] Sood, A.K., R.K. Ohdar, and S.S. Mahapatra, *Parametric appraisal of mechanical property of fused deposition modelling processed parts.* Materials & Design, 2010. **31**(1): p. 287-295.
[8] Dizon, J.R.C., et al., *Mechanical characterization of 3D-printed polymers.* Additive Manufacturing, 2018. **20**: p. 44-67.
[9] Mohamed, O.A., S.H. Masood, and J.L. Bhowmik, *Influence of processing parameters on creep and recovery behavior of FDM manufactured part using definitive screening design and ANN.* Rapid Prototyping Journal, 2017. **23**(6): p. 998-1010.
[10] Upadhyay, K., R. Dwivedi, and A.K. Singh, *Determination and Comparison of the Anisotropic Strengths of Fused Deposition Modeling P400 ABS*, in *Advances in 3D Printing & Additive Manufacturing Technologies*, D.I. Wimpenny, P.M. Pandey, and L.J. Kumar, Editors. 2017, Springer Singapore: Singapore. p. 9-28.
[11] Aliheidari, N., et al., *Interlayer adhesion and fracture resistance of polymers printed through melt extrusion additive manufacturing process.* Materials & Design, 2018. **156**: p. 351-361.
[12] Arivazhagan, A., S.H. Masood, and I. Sbarski. *Dynamic mechanical analysis of fused deposition modelling processed polycarbonate*. in *Annual Technical Conference - ANTEC, Conference Proceedings*. 2011.
[13] Domingo-Espin, M., et al., *Mechanical property characterization and simulation of fused deposition modeling Polycarbonate parts.* Materials & Design, 2015. **83**: p. 670-677.
[14] Montero, M., et al. *Material Characterization of Fused Deposition Modeling (FDM) ABS by Designed Experiments*. in *ANTEC 2011 Plastics: Annual Technical Conference Proceedings*. 2001.
[15] Susmel, L. and A. Ahmed, *A material length scale-based methodology to assess static strength of notched additively manufactured polylactide (PLA).* 2018.
[16] Ahmed, A.A. and L. Susmel, *Static assessment of plain/notched polylactide (PLA) 3D-printed with different infill levels: Equivalent homogenised material concept and Theory of Critical Distances.* Fatigue & Fracture of Engineering Materials & Structures, 2019. **42**(4): p. 883-904.
[17] Aliheidari, N., et al., *Fracture resistance measurement of fused deposition modeling 3D printed polymers.* Polymer Testing, 2017. **60**: p. 94.
[18] Zhang, W., et al., *Interfacial bonding strength of short carbon fiber/acrylonitrile-butadiene-styrene composites fabricated by fused deposition modeling.* Composites Part B: Engineering, 2018. **137**: p. 51-59.
[19] Caminero, M., et al., *Interlaminar bonding performance of 3D printed continuous fibre reinforced thermoplastic composites using fused deposition modelling.* Polymer Testing, 2018. **68**: p. 415-423.
[20] Anitha, R., S. Arunachalam, and P. Radhakrishnan, *Critical parameters influencing the quality of prototypes in fused deposition modelling.* Journal of Materials Processing Technology, 2001. **118**(1): p. 385-388.
[21] Salazar-Martín, A.G., et al., *A study of creep in polycarbonate fused deposition modelling parts.* Materials and Design, 2018. **141**: p. 414-425.
[22] D3518, *Standard Test Method for In-Plane Shear Response of Polymer Matrix Composite Materials by Tensile Test of a ±45° Laminate*. 2018, ASTM D3518/D3518M-18: ASTM International, West Conshohocken, PA.
[23] D3846, *Standard Test Method for In-Plane Shear Strength of Reinforced Plastics*. 2015, ASTM D3846-08: ASTM International, West Conshohocken, PA.
[24] BSS7260, *Advanced Composite Compression Tests*. 1988, Boeing Specification Support Standard BSS 7260: The Boeing Company, Seattle, Washington.
[25] D695, *Standard Test Method for Compressive Properties of Rigid Plastics*. 2015, ASTM D695-15: ASTM International, West Conshohocken, PA.
[26] Ngo, B.D., *Lab Report 1*. 2019, University of Technology Syndey: Sydney.
[27] Pilkey, W.D., *Peterson's stress concentration factors*. Third edition. ed, ed. D.F. Pilkey. 2008, Hoboken, New Jersey: Wiley.